

Chapter 2

Nonlinear Acoustic Waves in Layered Media

Abstract

In this chapter we investigate numerically the propagation of a plane acoustic wave in a periodic medium in a structured fluid, formed by a periodic array of fluid layers with alternating acoustic properties. Periodic acoustic media such as 1D layered media, or 2D sonic crystals, are known to introduce strong dispersion in wave propagation, even creating forbidden propagation bands or bandgaps where wave propagation at particular frequencies is not allowed. We show how the nonlinear generation and propagation of the second and higher harmonics are strongly affected by the presence of the periodicity. Thus, the combined action of nonlinearity (harmonic generation) and periodicity (different propagation velocities and attenuation for the different harmonics) results in novel and unexpected phenomena with respect to the linear counterpart, and opens the door to new mechanisms of acoustic wave control and manipulation.

2.1 Introduction

In the previous chapter we have considered waves propagating in nonlinear lattices. Such lattices can be macroscopic, idealized as masses coupled by springs, or even microscopic, as atoms/ions coupled by electromagnetic forces. Lattices can be then considered of basic model of solid matter, with its elements distributed periodically in a regular array. Many properties of solids, such as thermal conductivity, can be interpreted in terms of fundamental vibrations of the lattice, or phonons.

The study of matter as a periodic medium (a crystal of atoms), was originally performed by Bloch and Brillouin (Brillouin, 2003) in the 30-40's, and gave rise to an entire new discipline in physics, the solid state (or condensed matter) physics. One of the most celebrated effects of wave propagation in periodic media are the appearance of forbidden propagation regions in the energy spectrum of electrons, or band-gaps. Most of the physics of semiconductors, and therefore many electronic devices, are somehow based on this concept. In the late 80's, these ideas where extended by Yablonovich and John to light waves (electromagnetic waves in general) propagating in materials where the optical properties like the index of refraction were distributed periodically. These materials were named, by analogy with metals, as photonic crystals. The typical scale is given by the wavelength. Actually, not only light but any wave propagating in a periodic medium may experience the same effects, and acoustic waves are not an exception. Sound wave propagation in periodic media has become very popular in the last 20 years in acoustics, after the introduction of the concept of sonic crystals. Exploiting the analogies with other type of waves many interesting effects, as the mentioned forbidden propagation bands (band-gaps), but also focalization, self-collimation, negative refraction, and many others have been proposed. We consider in this chapter the simplest case plane waves propagating in a 1D structure, formed by a periodic alternation of layers with different properties. Depending on the context, such a structure has been named a multilayer, a superlattice (particularly in the context of semiconductors) or a 1D phononic crystal (this include more exotic structures, as the granular crystal or lattice).

The huge majority of the studies considered so far have assumed a low-amplitude (linear) regime, neglecting the nonlinear response of the medium. Intense wave propagation in nonlinear periodic media, and in particular the case of sound waves, is almost unexplored. In this chapter we present different examples of new phenomena related to sound wave propagation in multilayers, where each of the layer has a nonlinear cuadratic elastic response. Nonlinear acoustical effects in such structure have been studied only in a few works. For example, in (Yun et al., 2005) the harmonic generation process is described in a fluid/fluid multilayered structure (water/glicerine), based in a nonlinear wave equation. Also, acoustic solitons in solid layered nonlinear media have been presented (Yong et al., 2003). More recently, nonlinearity plus periodicity has been considered in (Liang et al., 2009), where an asymmetric propagation device (acoustic diode) was proposed.

There, the nonlinearity and the periodicity appear in different position and its effect is consider separately.

The effects discussed in this Chapter are the result of the interplay between nonlinearity and periodicity. We mostly concentrate in two phenomena: the control of harmonic distortion and the generation and propagation of solitons in the multilayer. The first case is analyzed in depth, and the conditions needed to selectively act on the nonlinearly generated spectrum, and therefore manipulate the waveform in the desired way, are obtained and discussed.

The theory in this Chapter has been developed for fluid-fluid (scalar) structures, however the main conclusions are extendable to fluid-solid or to solid-solid multilayers, if particular conditions are given. Also, the main conclusions in the Chapter are independent on the regime of the waves (audible, ultrasound,...), and therefore on the size or scale of the structure. However, there is a domain, when ultrasound waves reach the Teraherz regime, where these ideas may find a great potential. The progress in miniaturization and the technological development allows currently to create multilayers at scales even in the nanometer range (each layer contains then a small number of atoms). This structures are usually made of semiconductors and are often used in particular applications as phononic mirrors to form phonon nanocavities, (Huynh et al., 2006) or microcavities to obtain a strong optomechanical coupling (Fainstein et al., 2013) (for a revent survey, see Huynh et al. (2015)). Notably, acoustic amplification was realized in doped GaAs/AlAs superlattices and recently a saser, for sound amplification by the stimulated (acoustic phonons) radiation was demonstrated, in a device including a superlattice gain medium and GaAs/AlAs SLs acoustic mirrors (Maryam et al., 2013).

Some phenomena are common to lattices and superlattices (both are nonlinear, dispersive, periodic media), and the results of this Chapter and the previous are connected. Harmonic generation has been described in granular chains, modeled by FPU equation. Such quadratic FPU is actually a basic model for lattices with different interaction potentials (like Hertz, Coulomb,...) for small displacements. The continuous limit of this equation gives the nonlinear acoustic equation, which actually connects the propagation of sound waves with the microscopic theory of matter.

2.2 Dispersion relations

We consider the simple case of a 1D periodic medium made of an arrangement of homogeneous fluid media of thickness a_i with varying material properties. For the shake of simplicity only longitudinal waves under normal incidence are considered. A scheme of the system is shown in Fig. 2.1.

The propagation of small amplitude waves in an infinite periodic system is completely described by its dispersion relation, often known as band structure,

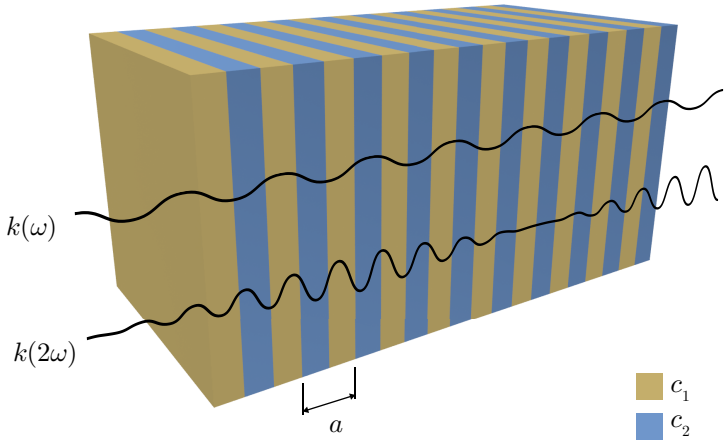


Figure 2.1: Layered acoustic system with two different layers and second harmonic generation scheme. Here the lattice period is $a = \sum a_i$.

that for 1D systems consisting in a periodic alternation of two different layers of length a_1 and a_2 can be expressed analytically as (Kosevich, 2005):

$$\cos(ka) = \cos(k_1 a_1)\cos(k_2 a_2) - \frac{1}{2}\left(\frac{k_1}{k_2} + \frac{k_2}{k_1}\right)\sin(k_1 a_1)\sin(k_2 a_2)\ , \qquad (2.1)$$

also known as the Rytov formula, where k is the Bloch wave-number, the lattice period is defined by $a = a_1 + a_2$ and $k_i = \omega/c_i$ with c_i the sound speed in the i layer. For a wave of frequency ω incident in a medium with known acoustical c_i and geometrical a_i parameters, the above equation results in a band structure of propagating and nonpropagating (bandgap) regions, as shown in Fig. 2.2. Thus, using Eq. (2.1), we can estimate the effect of periodicity on the different harmonics of the incident wave as they propagate trough the multilayer.

The ratio between layer thickness can be defined as

$$\alpha = a_1/a\,, \qquad (2.2)$$

leading to $a_2 = (1-\alpha)a$.

An example of dispersion relation plot is shown in Fig. 2.2 for normalized parameters $a = 0.5$ and for different sound speed ratios c_1/c_2. Increasing the impedance ratio between layers increases the reflected intensity in the trans-layer

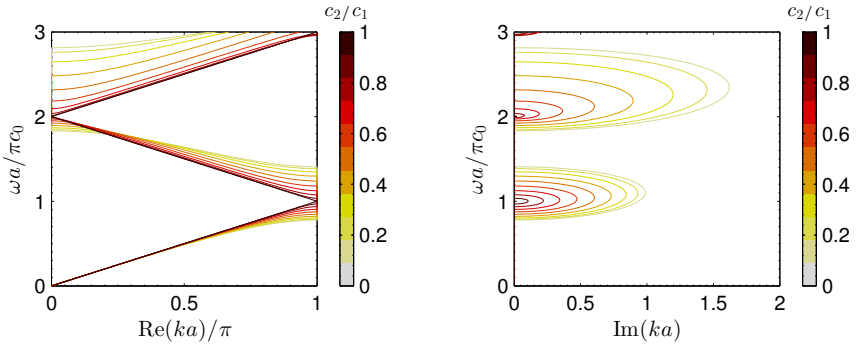


Figure 2.2: Dispersion relation of the two-layers system for layer proportion $\alpha = 0.5$ and for different c_2/c_1 ratio. Left: real wavenumbers. Right: imaginary part of the complex wavenumber.

propagation, while the transmitted energy of the multiple internal reflections diminishes. As can be seen, due to these scattering processes band-gaps are progressively open for wavenumber $k = n\pi/a$ with $n = 1, 2, ...$ Thus, the bandwidth of these band-gaps also increases when the impedance ratio grows.

On the other hand, its imaginary part increases in amplitude with c_1/c_2, leading to shorter evanescent propagation inside the band-gap for high sound speed contrast layers, while remains zero (no attenuation) in the propagation band. It is worth noting here that the system is conservative: the physical interpretation of the complex wavenumber is not energy absorption, but back reflection of the incident wave. Thus, at band-gap frequencies waves penetrate only a short distance into the medium with a forward evanescent mode, and if the medium is perfectly periodic and lossless the energy is back-reflected (it behaves as a mirror).

Furthermore, the curvature of the real part of the dispersion relations in the propagation band indicates dispersive propagation. However, in the low frequency regime the curve $\omega(k)$ is nearly linear. Here, a relation between c_1 and c_2 can be obtained for estimating the ratio in the limit $\omega \to 0$, $k \to 0$, that is the effective sound speed of the layered system $\tilde{c_0}$.

In order to obtain c_0 we first expand in Taylor series Eq. (2.1) in powers of ω around $\omega = 0$, and collecting terms up to second order we get

$$\omega \approx \sqrt{\left(1 - \cos\left(ka\right)\right) \frac{2c_1^2 c_2^2}{a\left(a_2 c_1^2 + a_1 c_2^2\right)}}. \tag{2.3}$$

Then, we expand again in Taylor series in powers of k around $k = 0$, and collecting terms up to first order we get

$$\tilde{c_0} = \frac{\omega}{k} \approx \sqrt{\frac{a c_1^2 c_2^2}{a_2 c_1^2 + a_1 c_2^2}}. \tag{2.4}$$

This value characterizes the layered media in the low frequency regime where the wavelength is much greater than the distance between layers. Furthermore, $\tilde{c_0}$ is useful also for frequency normalization, as long the first band-gap appears at $\omega = \pi\tilde{c_0}/a$ as can be appreciated in the common slope in the low frequency regime in Fig. 2.2. This quantity can be also obtained by assuming a mean density, $\tilde{\rho}$, and compressibility, $\tilde{\kappa}$ as (Yong et al., 2003):

$$\tilde{c_0} = \sqrt{\frac{\tilde{\kappa}}{\tilde{\rho}}}, \tag{2.5}$$

where the mean values for density and compressibility can be obtained as

$$\tilde{\rho} = \alpha\rho_1 + (1-\alpha)\rho_2\,, \tag{2.6}$$

$$\frac{1}{\tilde{\kappa}} = \frac{1}{\alpha\kappa_1} + \frac{1}{(1-\alpha)\kappa_2}, \tag{2.7}$$

being $\kappa_i = \rho_i c_i^2$ the compressibility of each layer.

2.3 Full-wave model

2.3.1 Nonlinear constitutive mode

The nonlinear propagation of sound in the acoustic inhomogeneous media, and in particular in multi-layered media can be described by several models, with different levels of accuracy. Here, we start from the equations of continuum mechanics for ideal fluids with space dependent parameters. Thus, applying mass conservation principle over a fluid control volume, the continuity equation reads (Naugolnykh et al., 1998):

$$\frac{\partial\rho}{\partial t} + \nabla\cdot(\rho\mathbf{v}) = 0\,. \tag{2.8}$$

On the other hand, the conservation of momentum over the same fluid test volume leads to the equation of motion

$$\rho\frac{D\mathbf{v}}{Dt} + \nabla p = 0\,, \tag{2.9}$$

where ρ is the total density, $\mathbf{v}$ is the particle velocity vector over a Eulerian reference frame, p is the acoustic pressure, t is the time and D is the material derivative operator

$$\frac{D}{Dt} = \frac{\partial}{\partial t} + \mathbf{v} \cdot \nabla \,. \tag{2.10}$$

For non homogeneous media, the ambient properties of the fluid in the absence of sound can be space dependent, so the total density becomes $\rho(t, \mathbf{x}) = \rho'(t, \mathbf{x}) + \rho_0(\mathbf{x})$, where $\rho_0(\mathbf{x})$ is the spatially dependent ambient density and $\rho'(t, \mathbf{x})$ is the perturbation of the density or acoustic density, that is space and time dependent. Then, using the material derivative, Eq. (2.9) becomes

$$\rho_0 \frac{\partial \mathbf{v}}{\partial t} + \nabla p = -\rho' \frac{\partial \mathbf{v}}{\partial t} - (\rho' + \rho_0)\,(\mathbf{v} \cdot \nabla)\,\mathbf{v} \,. \tag{2.11}$$

In this equation, the first two terms in the left-hand-side accounts for linear acoustic propagation, where the terms in the right-hand-side introduces nonlinearity in the Eulerian reference frame through momentum advection processes.

On the other hand, we can expand Eq. (2.8) for non-homogeneous media as

$$\frac{\partial \rho'}{\partial t} + \rho_0 \nabla \cdot \mathbf{v} + \mathbf{v} \cdot \nabla \rho_0 = -\rho' \nabla \cdot \mathbf{v} - \mathbf{v} \cdot \nabla \rho' \,. \tag{2.12}$$

Here, the first two terms on the left-hand-side account for linear acoustic propagation, the third, also linear, accounts for the magnitude of the changes in the ambient layer properties. Note this term is space dependent but only changes at the interface between adjacent layers. For density matched layers, $\rho_i = \rho_{i-1}$, this terms vanishes. The terms on the right-hand-side are nonlinear and accounts for mass advection. This equation remains exact.

Finally, a fluid thermodynamic state equation $p = p(\rho, s)$ is needed to close the system, with s the entropy. The local nonlinear media response relating density and pressure variations, retaining up to second order terms, can be written as

$$p = c_0^2 \rho' + \frac{B}{2A} \frac{c_0^2}{\rho_0} {\rho'}^2 \,, \tag{2.13}$$

where $B/A(\mathbf{x})$ is the quadratic nonlinear parameter and $c_0(\mathbf{x})$ is the sound speed, that can be also spatially dependent.

In this system of equations, quadratic nonlinearity appears in the equation of motion (2.11) and in the continuity equation (2.12), in the momentum and mass advection terms respectively, and also in the equation of state, Eq. (2.13), relating pressure and density acoustic perturbations. It is worth noting here that we only take into account nonlinear processes through the layer's bulk. The nonlinear effects at the boundary between adjacent sheets are neglected. These nonlinear boundary effects include cavitation processes, that in the case of fluids with very

different compressibility can be very important. In the case of solid layers, other local nonlinear effects relative to boundaries, e.g. clapping phenomena between surfaces, can lead to nonlinearities that are orders of magnitude in importance compared to the *bulk* cumulative nonlinearities (Tournat et al., 2004).

2.3.2 Second-order model

For moderate amplitudes, the system of Eq. (2.11-2.13) can be simplified. In the following, we use same ordering scheme as in Ref. Hamilton et al. (1998a), where $\mathcal{O}(\varepsilon)$, $\mathcal{O}(\varepsilon^2)$ and $\mathcal{O}(\varepsilon^3)$ represents the terms of generic smallness parameter ε. The derivation of a second-order nonlinear wave equation requires the substitution of the linearized acoustic approximations (first order) into second order terms of Eq. (2.12, 2.21). This substitution procedure will give third order errors, so the final nonlinear wave equation will be a second order approximation of the full constitutive relations.

Therefore, the first order equations of momentum and continuity can be obtained by linearization of Eq. (2.11-2.13) by assuming the acoustical magnitudes, ρ', p', and $\mathbf{v}$, are of small amplitude compared to the ambient values. Thus, for small amplitude perturbations the constitutive equations become

$$\frac{\partial \rho'}{\partial t} = -\rho_0 \nabla \cdot \mathbf{v} + \mathcal{O}(\varepsilon^2)\,, \tag{2.14}$$

$$\rho_0 \frac{\partial \mathbf{v}}{\partial t} = -\nabla p + \mathcal{O}(\varepsilon^2)\,, \tag{2.15}$$

$$\rho' = \frac{p}{c_0^2} + \mathcal{O}(\varepsilon^2)\,. \tag{2.16}$$

Then, we begin to manipulate the second order terms of the full constitutive relations with these first order approximations. Thus, using Eq. (2.14), the third right-hand-side term of the exact continuity Eq. (2.12) can be approximated up to second order as

$$-\rho' \nabla \cdot \mathbf{v} = \frac{\rho'}{\rho_0} \left(\frac{\partial \rho'}{\partial t} \right) + \mathcal{O}(\varepsilon^3)\,, \tag{2.17}$$

and using the linearized state Eq. (2.16) and rearranging terms leads to

$$-\rho' \nabla \cdot \mathbf{v} = \frac{1}{2\rho_i c_0^4} \frac{\partial p^2}{\partial t} + \mathcal{O}(\varepsilon^3)\,. \tag{2.18}$$

On the other hand, the fourth right-hand-side term of continuity Eq. (2.12) can be rewritten using the first order Eq. (2.15, 2.16) as

$$-\mathbf{v}\cdot\nabla\rho' = \frac{\rho_0}{2c_0^2}\frac{\partial u^2}{\partial t} + \frac{\mathbf{v}\rho'}{c_0^2}\nabla c_0^2 + \mathcal{O}(\varepsilon^3)\,. \tag{2.19}$$

Note that the last term of the above equation, that accounts for the local effect of the sound speed spatial variations, is $\mathcal{O}(\varepsilon^3)$, so it will be discarded, in contrast to the local effect of the ambient-density spatial variations (third term of Eq. (2.12)), that is $\mathcal{O}(\varepsilon^2)$ and it will remain in the derivation of the second order nonlinear wave equation for the layered media.

On the other hand, using the vector identity $(\mathbf{v}\cdot\nabla)\,\mathbf{v} = \frac{1}{2}\nabla v^2 - \mathbf{v}\times\nabla\times\mathbf{v}$ with $v^2 = \mathbf{v}\cdot\mathbf{v}$, and collecting terms up to second order, the equation of motion, Eq. (2.11), can be rewritten as

$$\rho_0\frac{\partial\mathbf{v}}{\partial t} + \nabla p = \frac{1}{2}\rho_0\nabla v^2 - \rho'\frac{\partial\mathbf{v}}{\partial t} + \rho_0\mathbf{v}\times\nabla\times\mathbf{v} + \mathcal{O}(\varepsilon^3)\,. \tag{2.20}$$

In general, although it is second order, the vorticity term (last term in the right-hand-side) decays exponentially away from rigid boundaries and can be discarded. However, it is essential to the analysis of other second order phenomena as the acoustic streaming (Hamilton et al., 1998a). In the following we will assume irrotational fluid. For a layered system, where the layer boundaries are orthogonal to the acoustic wave-vector, the vorticity modes can be neglected, while for strictly 1D propagation vanishes. Therefore, Eq. (2.20) becomes

$$\rho_0\frac{\partial\mathbf{v}}{\partial t} + \nabla p = -\frac{1}{2}\rho_0\nabla v^2 - \rho'\frac{\partial\mathbf{v}}{\partial t} + \mathcal{O}(\varepsilon^3)\,. \tag{2.21}$$

On the other hand, the second term of the right-hand-side of the above equation can be approximated up to second order using the first order Eqs. (2.14, 2.16) as

$$-\rho'\frac{\partial\mathbf{v}}{\partial t} = \frac{1}{2\rho_0 c_0^2}\nabla p^2 + \mathcal{O}(\varepsilon^3)\,. \tag{2.22}$$

Therefore, the second order approximation of the full constitutive relations in nonhomogeneous media can be expressed as:

$$\frac{\partial\rho'}{\partial t} + \rho_0\nabla\cdot\mathbf{v} + \mathbf{v}\cdot\nabla\rho_0 = \frac{1}{2\rho_0 c_0^4}\frac{\partial p^2}{\partial t} + \frac{\rho_0}{2c_0^2}\frac{\partial u^2}{\partial t} + \mathcal{O}(\varepsilon^3)\,, \tag{2.23}$$

and

$$\rho_0\frac{\partial\mathbf{v}}{\partial t} + \nabla p = -\nabla\left(\frac{1}{2}\rho_0 v^2 - \frac{1}{2\rho_0 c_0^2}p^2\right) + \mathcal{O}(\varepsilon^3)\,. \tag{2.24}$$

Using the definition of the Lagrangian density

$$\mathcal{L} = \frac{\rho_0}{2c_0^2}u^2 - \frac{p^2}{2\rho_0 c_0^2}, \tag{2.25}$$

the second order relations can be rewritten in a compact form

$$\frac{\partial \rho'}{\partial t} + \rho_0 \nabla \cdot \mathbf{v} + \mathbf{v} \cdot \nabla \rho_0 = \frac{1}{\rho_0 c_0^4}\frac{\partial p^2}{\partial t} + \frac{1}{c_0^2}\frac{\partial \mathcal{L}}{\partial t} + \mathcal{O}(\varepsilon^3)\,, \tag{2.26}$$

and

$$\rho_0 \frac{\partial \mathbf{v}}{\partial t} + \nabla p = -\nabla \mathcal{L} + \mathcal{O}(\varepsilon^3)\,. \tag{2.27}$$

These equations can be combined to form a unique nonlinear wave equation by subtracting the time derivative of Eq. (2.26) to the divergence of Eq. (2.26) to obtain

$$\nabla^2 p - \frac{\partial^2 \rho'}{\partial t^2} - \frac{\partial \mathbf{v}}{\partial t}\nabla \rho_0 = -\frac{1}{\rho_0 c_0^4}\frac{\partial^2 p^2}{\partial t^2} - \left(\nabla^2 + \frac{1}{c_0^2}\frac{\partial^2}{\partial t^2}\right)\mathcal{L} + \mathcal{O}(\varepsilon^3)\,. \tag{2.28}$$

Here, the third term can be expressed in terms of the acoustic pressure using the local instantaneous media response described by the state equation

$$\rho' = \frac{p}{c_0^2} - \frac{1}{\rho_0 c_0^4}\frac{B}{2A}p^2\,. \tag{2.29}$$

The fourth term of Eq. (2.28) can be also approximated using the first order Eq. (2.15), to finally obtain the second order nonlinear wave equation for nonhomogeneous media

$$\nabla^2 p - \frac{1}{c_i^2}\frac{\partial^2 p}{\partial t^2} - \frac{1}{\rho_0}\nabla \rho_0 \nabla p = -\frac{\beta}{\rho_0 c_0^4}\frac{\partial^2 p^2}{\partial t^2} - \left(\nabla^2 + \frac{1}{c_0^2}\frac{\partial^2}{\partial t^2}\right)\mathcal{L} + \mathcal{O}(\varepsilon^3)\,. \tag{2.30}$$

where we introduced the coefficient of nonlinearity $\beta = 1 + \frac{B}{2A}$ that accounts for material and mass advection quadratic nonlinearities. It is worth noting here (and discussed elsewhere (Hamilton et al., 1998a)) that the second-order Lagrangian density vanish for plane progressive waves due to the first order relation $p = uc_0\rho_0$ that leads to $\mathcal{L} = 0$. In this case, Eq. (2.28) simplifies to the well-known Westervelt equation for inhomogeneous media

$$\nabla^2 p - \frac{1}{c_0^2}\frac{\partial^2 p}{\partial t^2} - \frac{1}{\rho_0}\nabla\rho_0\nabla p = -\frac{\beta}{\rho_0 c_0^4}\frac{\partial^2 p^2}{\partial t^2} + \mathcal{O}(\varepsilon^3)\,. \tag{2.31}$$

In general, the Lagrangian density term can be discarded based on the distinction of cumulative and local nonlinear effects. In this way, for progressive quasi-plane wave propagation in homogeneous media the nonlinear local effects become insignificant in comparison to the nonlinear cumulative effects, where in most practicals situations, beyond a distance of only one wavelength away from the source local nonlinear effects can be neglected. However, local nonlinear effects can become significant in other complex situations including standing-wave fields. Concerning the layered media, in this Chapter we solve numerically the full constitutive relations, and we use the second order approximation Eq. (2.31) to obtain analytical solutions where the effect of the Lagrangian density term is assumed to be negligible.

2.3.3 Numerical solution

For one-dimensional acoustic waves $\mathbf{v} = (v_x, 0, 0)$, so the full constitutive relations Eqs. (2.8-2.11) can be expressed for nonhomogeneous media as

$$\frac{\partial \rho}{\partial t} = -\frac{\partial(\rho v_x)}{\partial x}\,, \tag{2.32}$$

$$\frac{\partial v_x}{\partial t} = -\frac{1}{2}\frac{\partial v_x^2}{\partial x} - \frac{1}{\rho}\frac{\partial p}{\partial x}\,, \tag{2.33}$$

The system of equations (2.13, 2.32-2.33) can be solved by several numerical methods (Botteldooren, 1996; Ginter et al., 2002; Vanhille et al., 2004; Albin et al., 2011). In this chapter we use the Finite-Differences in Time-Domain (FDTD) method: the density and pressure domain are discretized staggered in time and space respect to the particle velocity field, spatial and temporal derivatives are solved by centered finite difference operators, while the temporal integration is an explicit leap-frog scheme that consecutively solves density, pressure and particle velocity from continuity, momentum and state equations respectively. Thus, due to the 2-point stencil of the centered finite differences, the algorithm presents second order accuracy. Stability is achieved by the well-known Courant- Fiedrich-Levy (CFL) time step restriction and numerical FDTD dispersion is controlled due to a high enough grid refinement. Due to the low-dimensional space, a refinement > 100 elements per wavelength gives a negligible numerical dispersion compared to the physical one due to the layered system.

The dispersion relation (band structure) can be numerically obtained for the 1D system by a time-domain simulation of the linearized system. Linearization of

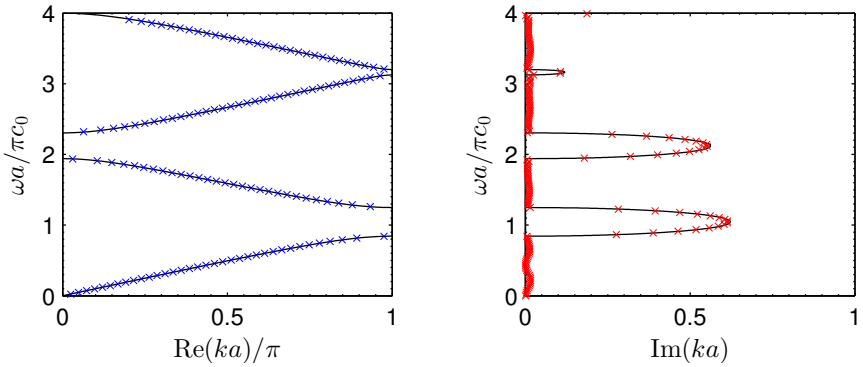


Figure 2.3: Dispersion relation of the two-layers system for normalized parameters $\alpha = 0.5$ and $c_2/c_1 = 0.5$. Left: real wavenumbers. Right: imaginary part. Rytov analytical Eq. (2.1) (Continuous line) and numerical solution (markers).

equations (2.13, 2.32-2.33) leads to the small amplitude version of Eq. (2.30), that is the nonhomogeneous wave equation, so both models present the exact same solution. Simulated pressure of Eqs. (2.13, 2.32-2.33) using a small amplitude excitation ($p_0 = 10^{-6}$ Pa or $\varepsilon = u_0/c_0 \approx 10^{-16}$) was recorded at two locations x_0 and x_1, located in different layers. Attenuation and phase velocity were estimated from the spectral components over the bandwidth of the recorded signals, that in this case was a numerical Dirac delta function in order to excite the entire numerical bandwidth. The numerical attenuation was calculated as

$$\alpha(\omega) = \frac{\ln\left(|P(\omega, z_2)/P(\omega, z_1)|\right)}{(z_1 - z_0)}\,, \tag{2.34}$$

where $P(\omega)$ is the Fourier transform of the measured pressure waveforms at points x_1 and x_2. On the other hand, the phase velocity was computed as

$$c_p(\omega) = \frac{\omega \cdot (z_2 - z_1)}{\arg\left(P(\omega, z_2)/P(\omega, z_1)\right)}\,, \tag{2.35}$$

where a correct phase unwrapping is needed in the arg function. Figure 2.3 shows the numerical and theoretical estimations of the dispersion relations, where excellent agreement is observed between them.

2.4 Harmonic generation in layered media

2.4.1 Overview

We start studying the response of the layered system for plane-harmonic wave excitation. Then, as sketched in Fig. (2.1), the source is placed in one boundary of the layered system, and the acoustic relevant magnitudes are calculated and measured along space and time. As the wave propagates, cumulative nonlinear effects generate harmonics of the fundamental frequency, ω_0, and due to the multiple scattering processes into the layers, local nonlinear effects also distorts the wave. However, the high dispersion of the layered system have a strong impact on the nonlinear harmonic generation. Dispersion modify the resonance conditions between fundamental and second harmonic wave, and also for other nonlinearly generated higher frequencies. In this way, nonlinear energy transfer efficiency from one component to another is modified in a wide variety of configurations, leading to the possibility of engineering and controlling the nonlinear wave processes by tuning the dispersion relation.

Figures 2.4 Figure 2.5 show an overview of the nonlinear harmonic generation over the propagation distance in a sample of layered media for normalized parameters $\alpha = 0.5$ and $c_2 = 0.7c_1$. From now on, if it is not explicitly said, the rest of the medium parameters are kept constant for the sake of simplicity, namely $\rho_1 = \rho_2$ and $B_1/A_1 = B_2/A_2$. If the frequency of the fundamental wave is varied, the harmonic generation exhibit various phenomena depending on the dispersion relation (plotted on the left of Fig 2.4a and Fig. 2.4b). Thus, we difference different frequency areas that will be explained below. It is worth noting here that the specific limiting frequency values and bandwidth between areas are strongly depending in the layered parameters However, the ordering of zones for different phenomena are, in general, the following:

(A) **Fubini-homogeneous**: The first zone is the very-low frequency band where the dispersion relation is nearly flat not only for the fundamental wave, but also for higher spectral components. In this region, the layered system behaves as an homogeneous material with effective parameters and dispersion can be neglected.

(B) **Weak-dispersion**: As the frequency is increased dispersion start to appear and different harmonics propagate with different wave speed. In the low dispersive regime, second harmonic dispersion is weak and even can be neglected, but third harmonic experiment strong dispersion and higher harmonics can fall in a band-gap where its propagation will be evanescent. Due to this situation, the energy transfer from the fundamental to its second harmonic is almost constant, and the second harmonic grows linearly with propagation. However, higher order cascade processes can be modified due to dispersion and the energy transfer from second to higher harmonics is decreased. This

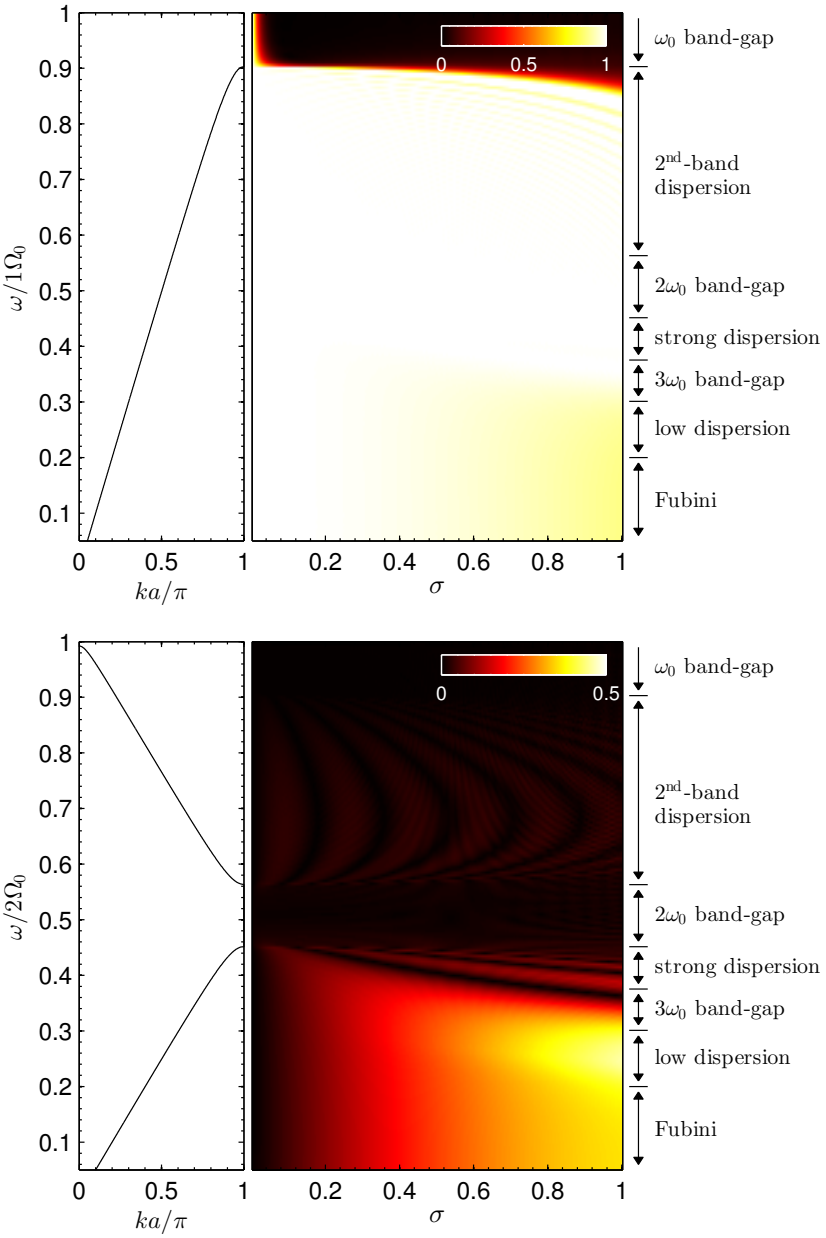


Figure 2.4: Overview of the harmonic generation processes in a nonlinear layered acoustic media. Top: fundamental component field, bottom: second harmonic field. Left: dispersion relation of the two-layers system for normalized parameters $\alpha = 0.5$ and $c_2/c_1 = 0.7$. Right: pressure amplitude (color) normalized to the source amplitude versus fundamental wave (ω) frequency and distance normalized to shock distance (σ)

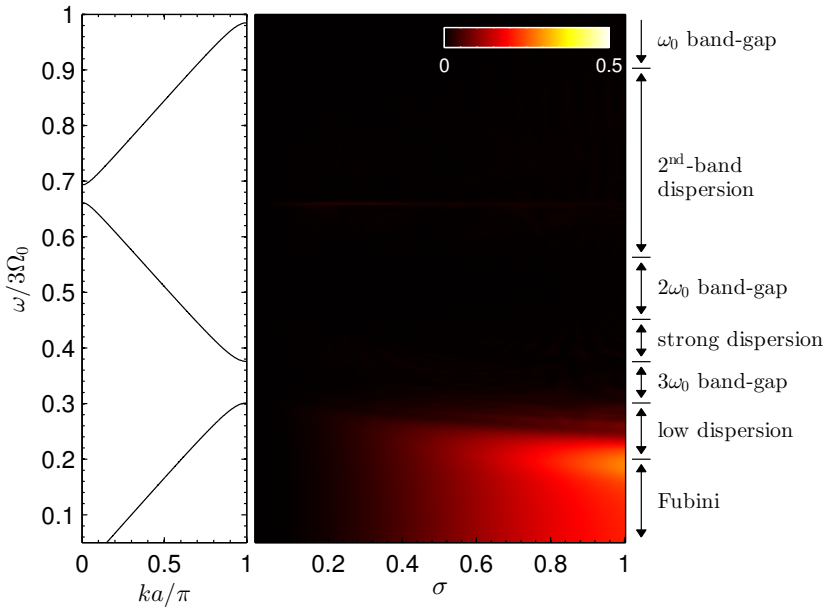


Figure 2.5: Overview of the harmonic generation processes in a nonlinear layered acoustic media for third harmonic. Left: dispersion relation of the two-layers system for normalized parameters $\alpha = 0.5$ and $c_2/c_1 = 0.7$. Right: pressure amplitude (color) normalized to the source amplitude versus fundamental wave (ω) frequency and distance normalized to shock distance (σ)

situation avoids the emergence of shocks and underthat conditions the second harmonic amplitude can overcomes the second harmonic field amplitude observed in the absence of dispersion.

(C) 3rd **harmonic in band-gap**: In this frequency area the propagation of third harmonic is evanescent and, in general, strong dispersion is observed on the second harmonic.

(D) **Strong-dispersion**: Where strong dispersion is observed for the second harmonic component, its field develops beatings in space, where its amplitude and spatial frequency depends on the matching conditions.

(E) 2nd **harmonic in band-gap**: In this frequency area second harmonic propagation is evanescent and the field does not grow with distance, but achieves a nearly constant value, being locally forced by the first.

(F) 2nd **band dispersion**: When second harmonic is in the second band, a high variability of phenomena can be observed depending on the material parameters. In the sample plot in Fig. 2.4 the second harmonic develops oscillations whose period varies by changing the frequency due to different phase matching conditions. By tuning material parameters and frequency different phase

matching conditions can be obtained, leading to a wide variety of possibilities. A sample is observed in Fig. 2.5 for $\omega_0 = 0.6\Omega_0$, where third harmonic falls in the limit of the second band-gap and also phase-matching is higher for third that for second harmonic, leading to third harmonic field higher than the second for this specific situation.

(G) 1st **harmonic in band-gap**: When fundamental frequency falls in the band-gap evanescent propagation is achieved and only local nonlinearities can be exited. However, due to the imaginary part of the wavevector inside the band-gap, that depends on the frequency, (see Fig. 2.3), the length of the exponentially decaying propagation inside the layered media can be tuned and therefore second harmonic can be produced at the beginning of the layered media while fundamental cannot propagate at the exist of the system.

These scenarios will be studied in the following subsections.

2.4.2 Homogeneous-Fubini

We start studying the rpropagation in the layered system for harmonic excitation in the very low frequency regime, where we assume that $ka \ll 1$ holds. As the Rytov's Eq. (2.1) predicts, in the very low frequency regime the slope of the $\omega(k)$ curve is nearly flat, and after sound speed normalization using using Eq. (2.4), the dispersion of the layered system should be negligible. Thus, the medium behaves as a continuum-lossless homogeneous material with effective parameters. This is known as the homogenization limit. However, attention should be paid here if the fluid compressibility highly differs between layers because the validity of the effective parameters may fail. It is the case, for example, of a liquid with gas inclusions (bubbly liquids) (Gurbatov et al., 2011).

In limit of low-frequency, the dispersion of all the spectral components is negligible, and they all propagate at nearly the same velocity. Thus, in the absence of dispersion and attenuation process, the system of Eq. (2.13, 2.32-2.33) can be reduced for harmonic-plane wave to a Burger's evolution equation expressed in traveling coordinates with effective parameters, namely $\tilde{c_0}$, $\tilde{\rho_0}$ and $\tilde{\beta}$. Therefore, the approximate evolution equation in terms of the acoustic pressure can be written as:

$$\frac{\partial p}{\partial t} + \tilde{c_0}\frac{\partial p}{\partial x} = \frac{\tilde{\beta}}{2\tilde{\rho_0}\tilde{c_0}^2}\frac{\partial p^2}{\partial t}. \tag{2.36}$$

An analytic solution of this equation is also available through the Fubini's representation for the nth-harmonics of the fundamental wave of frequency ω and initial amplitude p_0 as

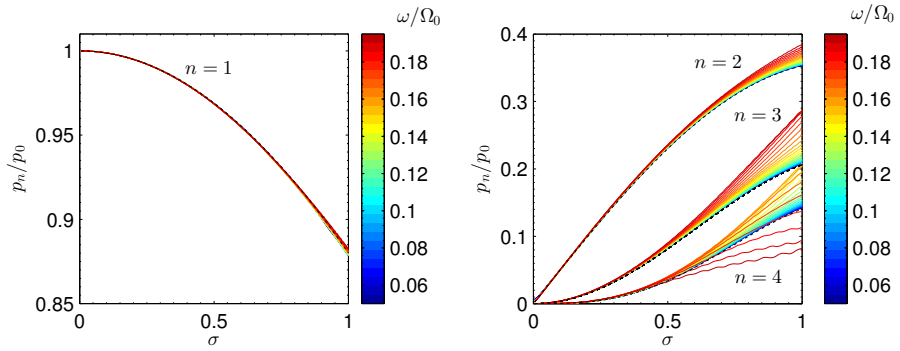


Figure 2.6: Harmonic generation in homogeneous-Fubini regime of the layered media

$$p(\sigma,\tau) = p_0 \sum_{n=1}^{\infty} \frac{2}{n\sigma} J_n(n\sigma)\sin(n\omega\tau), \tag{2.37}$$

where J_n is the Bessel function of order n, and $\sigma = x/x_s$ is the propagation coordinate, normalized to the shock formation distance:

$$x_s = \frac{1}{\tilde{\beta}\tilde{\varepsilon}k}, \tag{2.38}$$

with the effective match number $\tilde{\varepsilon} = u/\tilde{c_0}$ and the effective wavenumber $k = \omega/\tilde{c_0}$, that can be also found from Eq. (2.1). This celebrated solution is valid for $\sigma < 1$ (pre-shock region).

Simulations in this regime were carried out using a full-wave constitutive relations solver. Thus, we shall define the normalized frequency as $\Omega_0 = \pi\tilde{c_0}/a$ (located in the first band-gap). Therefore, the source frequency was set to $\omega = 0.1\Omega_0$.

Figure 2.6 shows the analytical and numerical solutions for the low frequency limit of the layered system, where an excellent agreement is obtained between Fubini and numerical solutions in the pre-shock region, $\sigma < 1$ and for low excitation frequencies. As commented above, when the fundamental frequency is increased the higher harmonics fall in dispersive region of the frequency bands, and thus its wave speed is reduced. In this situation, phase matching conditions are no longer fulfilled and therefore the energy transfer from fundamental to higher harmonics is modified. Thus, the Fubini solution can be only applied as an ideal solution for the low-frequency limit or as a good approximation for the first harmonics and for frequencies below $\omega \lesssim 0.1\Omega_0$.

However, it should be noted that for observing a shock wave, i. e. a discontinuous solution, all the spectral components must be phase matched, as occurs in

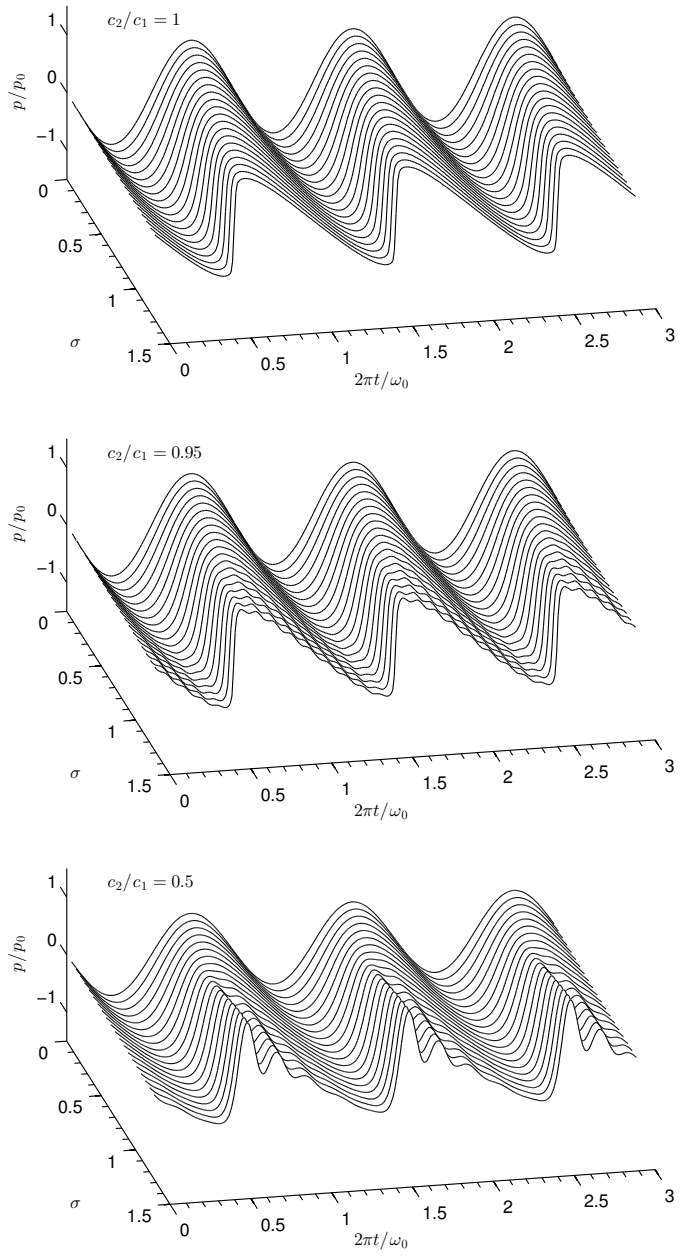


Figure 2.7: Waveform evolution beyond shock formation distance in layered media with parameters $\omega_0/\Omega_0 = 0.1$ and $c_2/c_1 = 1$ (top), $c_2/c_1 = 0.95$ (middle) and $c_2/c_1 = 0.5$ (bottom). Instead a discontinuity, pulsations around the sharp front are formed.

the nondispersive (homogeneous) media. Then, even for a low finite fundamental frequency, a small (but non negligible) dispersion will appear for the higher frequency components, and a phase mismatch is introduced on these high spectral components. The differences on phase speed on the different spectral components over a discontinuity impedes the formation of a stable traveling shock wave, as long sound speed dispersion spreads the high-frequency wave vectors that describe the discontinuous solution. Instead of a shock wave, pulsations or ripples are formed over the sharp nonlinear wavefront for $\sigma > 1$. This scenario reduces the validity of the homogeneous Eq. (2.36) to distances shorter than shock formation in lossless media, where the specific limit is dependent on the flatness of the dispersion relation near the band-gap, i.e. the layered media parameters: a, c_2/c_1, ρ_2/ρ_1 and $\alpha = a_1/a$.

Figure 2.7 shows the waveform evolution calculated at different distances in the shock-free region and also beyond shock formation distance for a homogeneous media ($c_2/c_1 = 1$) for a nearly-flat dispersion relation ($c_2/c_1 = 0.95$ and $\alpha = 0.5$) and for a more dispersive media ($c_2/c_1 = 0.5$, $d_2/d_1 = 0.5$). The above described effects are clearly visible: the waveform evolution follows the Fubini analytical solution for $\sigma < 1$ in both layered systems. However, for longer distances, pulsations around the discontinuity are formed due to different phase speed of the higher spectral components, spreading the sharp solution into a *solitonic* pulsations. In the absence of dissipation, these pulsations evolves in a train of weakly interacting solitons. Solitons in the layered media will be studied later on Sec. 2.6.

2.4.3 Dispersive regime

For frequencies above the (idealized) homogeneous-Fubini regime, finite (weak and strong) dispersion effects are observed. The dispersive effects of the layered system deeply affects harmonic generation processes.

As intense waves propagate through a quadratic nonlinear medium, their frequency component interact with each other and new frequencies arise at combination frequencies, including higher harmonics. The cumulative energy transfer from the interacting waves to the harmonics is dependent on the resonance conditions:

$$\omega_1 \pm \omega_2 = \omega_3 \ , \ \mathbf{k}_1 \pm \mathbf{k}_2 = \mathbf{k}_3. \tag{2.39}$$

Note these conditions express the laws of conservation of energy ($\hbar\omega$) and momentum ($\hbar\mathbf{k}$) in the quantum description for the disintegration and merging of quanta (Naugolnykh et al., 1998).

These conditions can be satisfied in a variety of situations. The most simple case is observed in nondispersive media and for collinear waves $k_i = \omega_i/c_0$. In this situation the resonance conditions are fulfilled all over the spectra and a large number of harmonics interacts synchronously: when there exist in the system a *free*

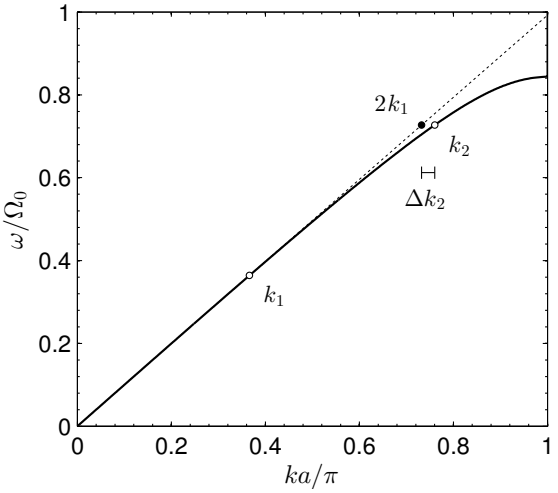


Figure 2.8: Scheme of the phase miss-matching situation. The fundamental wave vector k_1 at frequency ω generates a *forced* wave $2k_1$ at frequency 2ω. The *free* wave that the system allows to propagate is k_2, located in the dispersion relation curve. Due to dispersion, $k_2 \neq 2k_1$, thus there exist a phase mismatch, Δk_2 between both waves and the generation is therefore asynchronous.

wave with velocity $\omega_3/|\mathbf{k}_3|$ that matches the excited (*forced*) wave $\omega_1 \pm \omega_2/|\mathbf{k}_1 \pm \mathbf{k}_2|$, the *free* wave is excited in a resonant way. The resonant interaction leads therefore to synchronous, cumulative energy transfer from the initial wave to the secondary wave fields.

In the case of an initial monochromatic wave, the main wave generates its second harmonic. The resonant conditions Eq. (2.39) in this situation read

$$2\omega_1 = \omega_2 \ , \ 2\mathbf{k}_1 = \mathbf{k}_2, \tag{2.40}$$

that holds true for nondispersive collinear waves, leading to the simple relation $2\mathbf{k}(\omega_1) = \mathbf{k}(2\omega_1)$. However, in the case of dispersive media this condition is, in general, not fulfilled and the *forced* and *free* waves interact asynchronously. Figure 2.8 shows a scheme of this situation for a layered media with a fundamental wave in the first dispersion band.

In order to study asynchronous second harmonic generation processes, we recall here for the lossless second-order wave equation Eq. (2.31) for one-dimensional propagation

$$\frac{\partial^2 p}{\partial x^2} - \frac{1}{c_0^2}\frac{\partial^2 p}{\partial t^2} - \frac{1}{\rho_0}\frac{\partial \rho_0}{\partial x}\frac{\partial p}{\partial x} = -\frac{\beta}{\rho_0 c_0^4}\frac{\partial^2 p^2}{\partial t^2}. \tag{2.41}$$

This equation does not include dispersion by itself, dispersion arises from the solution of the linearized wave equation with the layered media boundary conditions, where the eigenvalue problem leads to the Rytov's dispersion relation Eq. (2.1).

In the following, we apply a perturbation method to obtain an approximate solution for the second harmonic field. We expand the pressure field as sum of contributions of different orders, as

$$p = p^{(1)} + \varepsilon p^{(2)} + \cdots , \tag{2.42}$$

where ε is the smallness perturbation parameter, which we identify with the acoustic Match number. Thus, $p^{(1)}$ is the first order (linear) solution of the problem and $p^{(2)}$ its the second order contribution. By substituting Eq. (2.42) in the second order wave Eq. (2.41), assuming constant density[1] and neglecting $\mathcal{O}(\varepsilon^3)$ terms we get the coupled set of equations

$$\frac{\partial^2 p^{(1)}}{\partial x^2} - \frac{1}{c_0^2}\frac{\partial^2 p^{(1)}}{\partial t^2} = 0 , \tag{2.43}$$

$$\frac{\partial^2 p^{(2)}}{\partial x^2} - \frac{1}{c_0^2}\frac{\partial^2 p^{(2)}}{\partial t^2} = -\frac{\beta}{\rho_0 c_0^4}\frac{\partial^2 p^{(1)2}}{\partial t^2}. \tag{2.44}$$

The first order Eq. (2.43) for a monochromatic plane wave of frequency ω has the trivial solution

$$p^{(1)} = p_0 \sin\left(\omega t - k_1 x\right) , \tag{2.45}$$

where $k_1 = k(\omega)$ is the wave vector associated with the primary frequency ω, and p_0 is the excitation pressure amplitude. Substitution of Eq. (2.45) into the right-hand side term of Eq. (2.44), using the trigonometric identity $\sin^2(\theta) = (1 - \cos(2\theta))/2$, an inhomogeneous equation for the second harmonic field is obtained:

$$\frac{\partial^2 p^{(2)}}{\partial x^2} - \frac{1}{c_0^2}\frac{\partial^2 p^{(2)}}{\partial t^2} = -\frac{4\beta\omega^2 p_0^2}{\rho_0 c_0^4}\sin\left(2\omega t - 2k_1 x\right). \tag{2.46}$$

The general solution of the this equation will be the sum of the solution of the homogeneous equation ($p_0 = 0$), and the particular solution of the inhomogeneous equation ($p_0 \neq 0$). Therefore the field for the second harmonic can be expressed as $p^{(2)} = p_h^{(2)} + p_f^{(2)}$, where the corresponding waves for this two solutions are the *free*, and *forced* waves respectively. Following Ref. Rudenko et al. (1977), we can obtain the homogeneous and particular solutions as:

[1] We neglect the ambient density variations for the sake of simplicity. Dispersion arise also for sound speed variations, that are assumed to be implicit in the boundary conditions.

$$p_h^{(2)} = p_h^{(2)}(x=0)\sin(2\omega_1 t - k_2 x), \tag{2.47}$$

$$p_f^{(2)} = \frac{A}{(k_2+2k_1)(k_2-2k_1)}\sin\left(2\omega_1 t - 2k_1 x\right), \tag{2.48}$$

where $k_2 = k(2\omega_1)$ is the wavenumber of the *free* wave at second harmonic frequency, and the constant $A = -4\beta\omega_1^2 p_0^2/\rho_0 c_0^4$. It is worth noting here that as long $2k_1 \neq k_2$, the *forced* and *free* waves in dispersive media have different phase speed, i. e. the *forced* and *free* waves are phase mismatched as can be seen in the argument of the sin function in Eq. (2.47-2.48). On the other hand, as long as there is not second harmonic at $x = 0$ (boundary condition), we must set

$$p_h^{(2)}(x=0) = -\frac{A}{(k_2+2k_1)(k_2-2k_1)}. \tag{2.49}$$

Therefore, combining Eqs. (2.47-2.49) the evolution of the second harmonic field can be expressed as

$$p^{(2)} = \frac{A}{k_2\Delta k}\sin\left(\frac{\Delta k}{2}x\right)\cos\left(2\omega_1 t - k_2' x\right), \tag{2.50}$$

where the effective wave number is $k_2' = (k_2 + 2k_1)/2 \approx k_2$ and the detuning parameter that describes the asynchronous second harmonic generation is defined as

$$\Delta k = |k_2 - 2k_1| = |k(2\omega) - 2k(\omega)|. \tag{2.51}$$

Equation (2.50) describes the well-known effect in second harmonic generation, that is the beatings in space of the second harmonic field when the resonant conditions are not fulfilled. Thus, as Δk increases, the beating spatial period and also its maximum amplitude decreases. The position of the maximum of the beating, also called the coherence length, can be related to the second-harmonic phase-mismatching frequency as

$$x_c = \frac{\pi}{\Delta k} = \frac{\pi}{|k(2\omega) - 2k(\omega)|}. \tag{2.52}$$

This length corresponds to the half of the spatial period of the beating, where the maximum of the field is located. It can be expressed also for other higher harmonics simply as $x_c(n) = \pi/\Delta k_n = \pi/|k(n\omega) - nk(\omega)|$.

In the limiting case of $\Delta k \to 0$, the second harmonic field is generated synchronous and accumulates with distance, so linear growth is predicted. In this

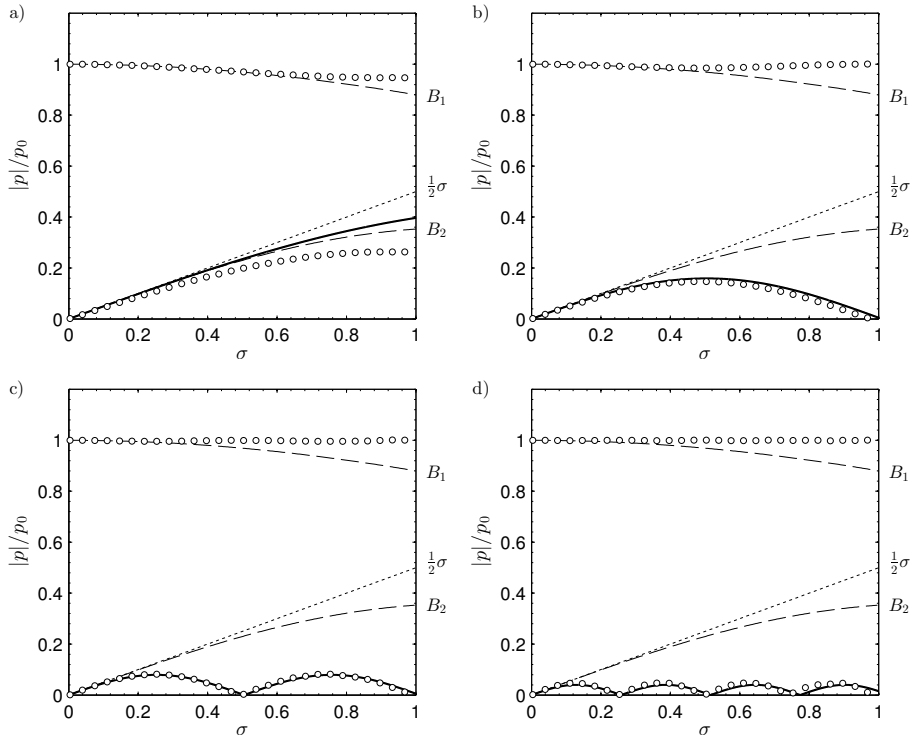


Figure 2.9: Second harmonic evolution for $x_c/x_s = [1, 1/2, 1/4, 1/8]$ obtained using Eq. (2.50) (continuous line), numerically (white circles), nondispersive linear law of growing (dotted line) and Bessel-Fubini nondispersive solution (dashed).

case, phase matching conditions are fulfilled and the *free* wave is excited synchronous to the *forced wave*. Note here that in the derivation of Eq. (2.50) only second order processes are taken into account and therefore, only second harmonic is predicted. This leads to overestimate the second harmonic field: as long no energy is transferred to third harmonic, second harmonic predicted by Eq. (2.50) in the absence of dispersion grows indefinitely. The validity of this model can be explored expanding the Bessel functions of Fubini series near the source. A simple comparison between the full Fubini solution and linear second harmonic growth gives a reasonable approximation for distances $\sigma < 0.5$ or for second harmonic field values of $p(2\omega) < p_0/4$.

Figure 2.9 shows four different simulations in the dispersive regime of the layered media where the wave amplitude and frequency has been selected to match $x_c/x_s = [1, 1/2, 1/4, 1/8]$. The higher beating spatial period waves corresponds to lower frequencies. The analytical solution for the second harmonic matches the full-wave numerical solution. However, differences can be observed in the second harmonic amplitude estimation for $x_c/x_s = 1$ (left plot in Fig. (2.9)). This

overestimation by the analytical solution can be related to the absence of energy transfer to higher harmonics, that is not considered by the perturbation solution but is included in the simulation. Therefore, this model is specially suitable in situations where the third harmonic does not grow cumulative with distance. In the lossless layered media, this situations include frequencies that leads to very high-third harmonic detuning and also when the third harmonic falls in band gap.

2.4.4 Second harmonic in band gap

Waves with frequencies falling into the band-gap of the dispersion relation are evanescent due the non negligible imaginary part of its complex wave number. Thus, its amplitude decays exponentially with distance. When the second harmonic frequency falls into the band-gap, a characteristic effect, studied also in other nonlinear lattices (Sánchez-Morcillo et al., 2013) can be observed: its amplitude reaches a constant value. Figure 2.10 present an example of this case for four

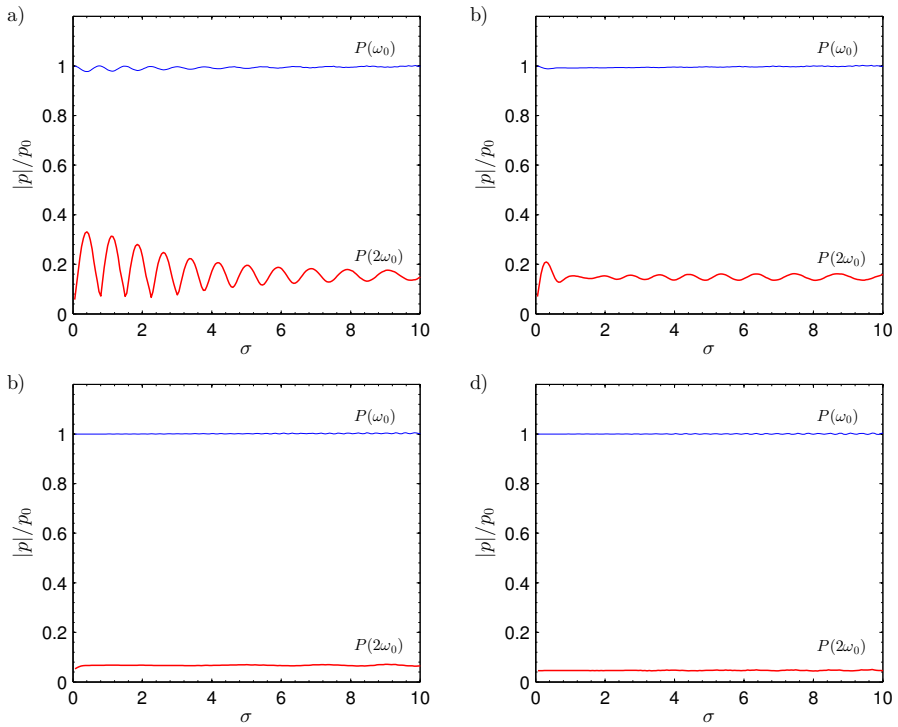


Figure 2.10: Evolution of the second harmonic field propagating in bang-gap for second harmonic frequencies (a) just above band-gap $2\omega_0 = 0.84\Omega_0$, (b) $2\omega_0 = 0.85\Omega_0$, (c) in the middle of the bandgap $2\omega_0 = \Omega_0$ and (d) $2\omega_0 = 1.05\Omega_0$ at the maximum of the imaginary part for the first band gap. All results for a layered system of $\alpha = 1/2$ and $c_1/c_2 = 1/2$.

different frequencies, where can be observed that the constant value of the second harmonic field depends on the imaginary part of the wave vector.

This effect can be understood in terms of the *free* and *forced* waves. If the second harmonic is evanescent (as follows from the dispersion relation), the wave will not accumulate with distance. But the fundamental wave is still "pumping" energy to the second harmonic field at every point in space. Thus, the second harmonic field is generated locally and remains trapped inside the layered media. It reaches a constant level that depends on three main factors. In first place, the "pumping" rate, characterized by the fundamental wave amplitude and medium nonlinearity, or more strictly the ratio between the layer thickness and the shock distance d/x_s. Secondly, it also strongly depends on the magnitude of the imaginary part of the complex wave number, i.e. the ratio between its characteristic exponential decay length and the shock distance in a layer. The characteristic decay length of the evanescent propagation is always shorter when the second harmonic is in the middle of the band-gap, leading to less second harmonic field in this frequency region, as can be seen in Fig. 2.10 (c-d). Finally, it depends also on the detuning of real part of the wave number, where for the first band-gap is minimum at the center. The first factor can be isolated and studied separately. However, the two last factors are linked through the specific dispersion relation of the medium.

Figure 2.11 shows the detuning of the second harmonic and the imaginary part as a function of the frequency for a medium with $\alpha = 1/2$ and $c_1/c_2 = 1/2$, showing that at the middle of the band-gap these two factors have opposite effects: detuning is minimized when evanescence decay is maximized and vice versa. However, the magnitude of the effects can be very different. As the rate of the second harmonic generation (see the initial slope in Fig. 2.9) is independent on the detuning, and the evanescence implies that the wave decays after few layers, there not exist a practical

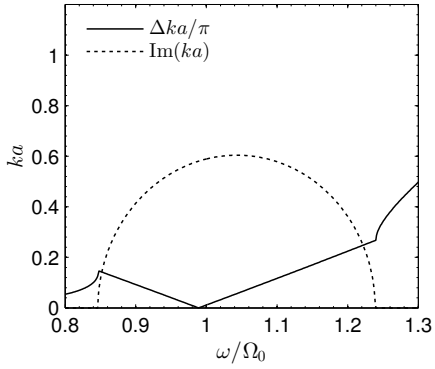


Figure 2.11: Detuning of the second harmonic (continuous line) and imaginary part (dotted line) in function of the normalized frequency.

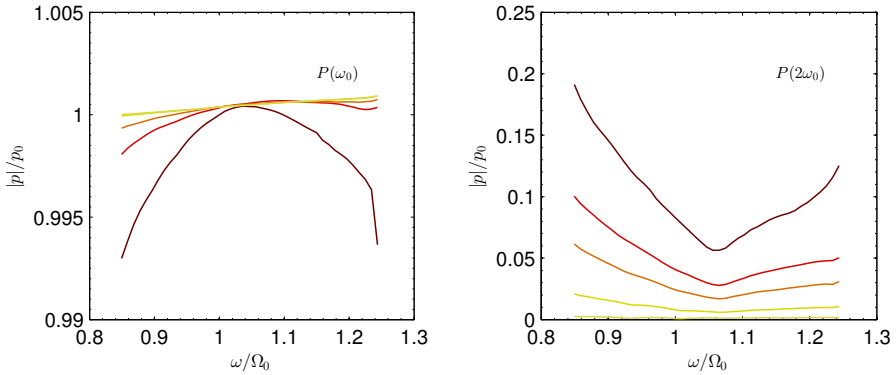


Figure 2.12: (left) Amplitude of the constant field value for fundamental (dashed) and (right) its second harmonic field (continuous line) for amplitudes matching $a/x_s = 0.08, 0.04, 0.02, 0.001$

compensation of the effects at the center of the band-gap. However, the situation is different for frequencies around the limits of the band-gap, where the coherence length is of the order of the exponential decay characteristic length. Thus, for frequencies just above bad-gap and for amplitudes with shock distance comparable to the evanescent characteristic decay length, the beatings can be also observed, as shown in Fig. 2.10 (a). Then, if frequency is increased the characteristic decay length becomes shorter than the shock wave distance and beatings cannot be observed, leading to to the characteristic constant second harmonic field shown in Fig. 2.10 (c-d).

Figure 2.12 (right) shows the second harmonic amplitude (of the constant field) in function of the frequency for different amplitudes matching a/x_s =0.08, 0.04, 0.02, 0.001, where it is clearly visible that the minimum field value is obtained at the frequency of the maximum imaginary part of the complex wave number. On the other hand, as more energy is transferred to second harmonic the fundamental amplitude decays in an inverse way of its second harmonic field, as shows in Figure 2.12 (left).

2.4.5 Fundamental harmonic in band gap

When the fundamental frequency of the wave lies within the band-gap, small amplitude waves propagates evanescently. Essentially, the same applies to finite amplitude harmonic waves. In general, if the shock distance is large compared to the exponential characteristic length of the evanescent wave, the nonlinear effects have no time to accumulate and harmonic amplitude is negligible. Since the characteristic exponential decay is about few lattice sites, this means that the initial amplitudes necessary to achieve nonlinear effects in this configuration are much higher than those in the preceding sections. Figure 2.13 shows the evolution of the

first and second harmonics for a fundamental frequency falling in the middle of the bad-gap, $2\omega_0 = 1\Omega_0$, and with a frequency just above but into the band-gap, $\omega_0 = 0.87\Omega_0$ for a layered media of $\alpha = 1/2$ and $c_1/c_2 = 1/2$. In the first case, the imaginary part of the wave vector is remarkable high and the waves decay fast after few lattice units. Due to this fast decay, the second harmonic interacts over a short distance with the first, and its amplitude is very limited. After few lattice units, fundamental wave can be treated as a small-amplitude evanescent-wave. The second harmonic, that also falls in bandgap (but in the second band) also decays exponentially.

On the other hand, if the fundamental frequency is set just above the band-gap, where the imaginary part of the wave-vector is smaller, the amplitude of the fundamental wave decays more slowly, penetrating deeper into the material. The interaction region with the second harmonic is larger, and nonlinear effects resultv in a more efficient generation of the second harmonic. Furthermore, as long the different (higher order) bandgaps in the layered media can have different band-width, in this configuration at $\omega_0 = 0.87\Omega_0$ second harmonic does not fall inside a bandgap. Therefore, the generated second harmonic wave at the beginning of the lattice propagates through the medium essentially without amplitude change. Due to the evanescence of the fundamental wave, there is only *forced* wave at the beginning of the medium. Therefore, although in this configuration waves are phase mismatched, beatings are not present: only the *free* wave propagates through the medium.

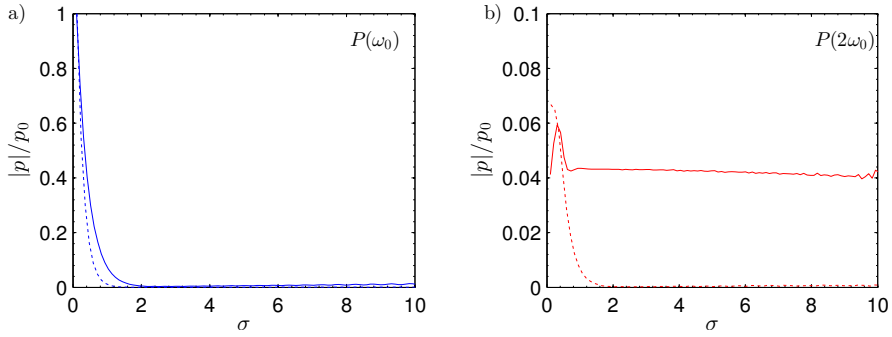


Figure 2.13: (a) Evolution of the fundamental harmonic wave field with its fundamental frequency falling just above into band-gap, $\omega_0 = 0.87\Omega_0$, (continuous line), and in the middle of the bad-gap, $2\omega_0 = 1\Omega_0$ (dotted line). (b) Corresponding second harmonic field, where for $\omega_0 = 1\Omega_0$ (dotted line) second harmonic frequency falls in the 2nd band band-gap while for $\omega_0 = 0.87\Omega_0$, (continuous line) lies into a propagating band.

2.5 Nonlinear acoustic field management

2.5.1 Tuning nonlinearity with dispersion

In the preceding sections we have explored the fundamental behavior of nonlinear waves generated inside layered media. However, the layered medium parameters can be tuned to provide specific conditions. These conditions are, among others, looking for detuning or coherence at specific frequencies and using the evanescent propagation in the bad-gap for another specific frequency.

The material parameters can be tuned to get coherence at one frequency of interest, e.g. at one of the harmonics of the fundamental wave, or to get detuning or evanescent propagation at other specific harmonics. Using these mechanisms the layered system provides a control of the nonlinear process inside the medium. Thus, the layered media can be tuned in order to obtain specific balance of the harmonic amplitude or specific nonlinear waveforms.

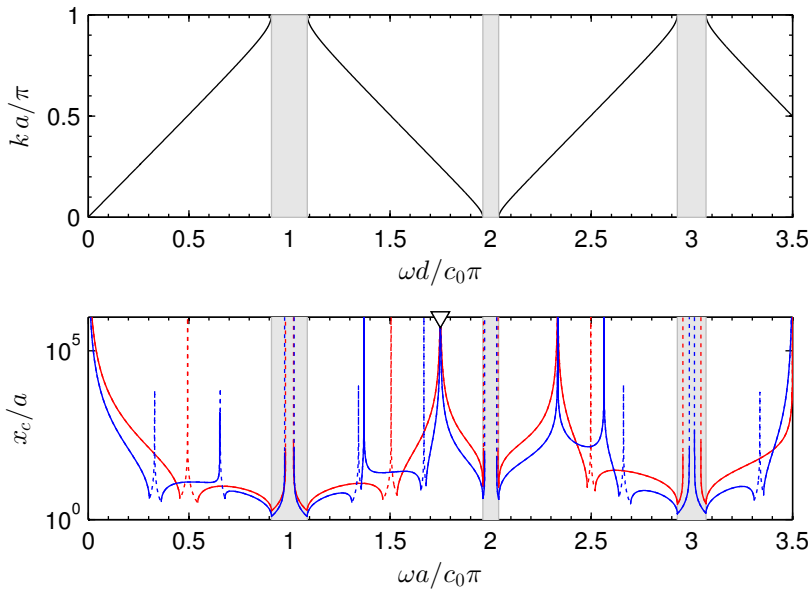


Figure 2.14: (Top) dispersion relation for a layered media of $c_1/c_2 = 1.33$ and $\alpha = 1/2$. (Bottom) coherence length for second (red) and third (blue) harmonic in function of the fundamental frequency. Phase matched frequencies are those with $x_c \to \infty$, while asynchronous generation is predicted for $x_c \to 0$. Frequencies at which the fundamental frequency is in band-gap are is marked in gray regions, while band-gap regions for second and third harmonic are marked in dashed lines.

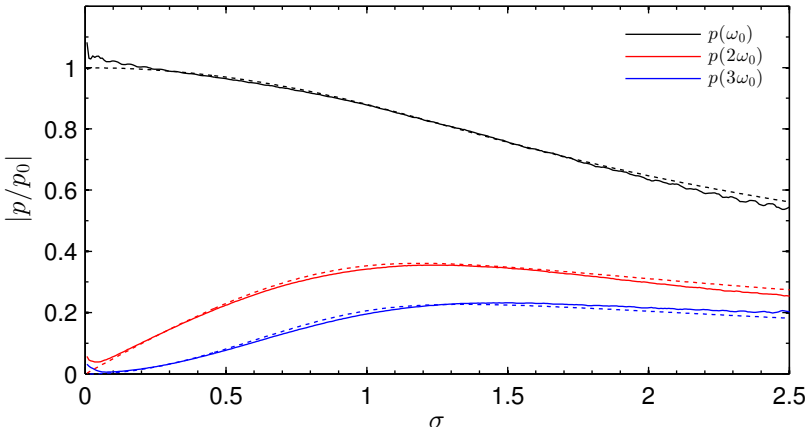


Figure 2.15: Harmonic distribution for the frequency $\omega_0 = 1.75/\Omega$. Coherence is recovered for at least the lowest spectral components. Blackstock solution (dotted lines).

In the design of a system for this purpose, the coherence length is a useful control parameter. Thus, Fig. 2.14 (top) shows an example of the dispersion relation with parameters $c_1/c_2 = 1.333$ and $a = 1/2$. Then, in Fig. 2.14 (bottom) the coherence length for the second and third harmonic is shown. The propagating bands are marked with continuous lines while the band-gap frequencies are marked in dotted lines. Thus, the abscissa axes marks the frequency of the fundamental wave. It can be observed that there exist singular frequencies, e.g. frequencies where all the harmonics are phase matched, $x_c \to \infty$. In Fig. 2.14 it happens for $\omega_0 = (0, 1.75, 2.333, ...)/\Omega$. On the other hand, there also exist frequencies at which there exist coherence for the second but a non-negligible detuning is observed for the third. Opposite effect can be observed, where coherence is achieved for the third harmonic but second harmonic presents strong dispersion. Finally, other interest regions are those where second harmonic component is almost phase matched and for the same frequency third harmonic falls into a band-gap.[2]

Thus, the analytic Eq. (2.1) provides an excellent framework to tune-up the layered parameters to obtain the desired balance between detuning, evanescent propagation, synchronous generation and, at the same time, it allows to find those conditions for a specific phase/group speed.

We start studying the harmonic distribution for an initial monochromatic wave of $\omega_0 = 1.75/\Omega$, corresponding to the triangle marked in Fig. 2.14 (bottom). Figure 2.15 shows the harmonic distribution, where, as expected, synchronous cumulative harmonic generation inside the dispersive media is recovered. The harmonic evolution in the second band follows again the Bessel-Fubini-Blackstock harmonic

[2]This singular situations can be also obtained with no difficulty for physical values of sound speed and other layer proportions. We use here normalized values for the sake of simplicity.

distribution for the lower spectral components. However some remark must be underlined. First, there exist some detuning for the high frequency components that avoids the formation of shock waves for $\sigma > 1$. Figure 2.16 shows the waveforms measured at $\sigma = (0.5, 1, \pi/2, 2)$. It can be observed that, although second and third harmonics are phase matched a shock is not produced. Due to finite detuning of the higher harmonic components, oscillations instead of a shock wave profile appears for $\sigma > 1$, as those presented in the low frequency limit in Sec. 2.4.2.

It is worth noting here that coherence is achieved in theoretically lossless media for all spectral components. However, losses can modify the dispersion relation specially for frequencies near the band-gap. Thus, in practical cases, where losses exist and typically increases quadratically with frequency, the dispersion relation will be modified specially at frequencies of the higher spectral components. In the presented cases, due to the introduction of some amount of artificial attenuation necessary for nonlinear numerical stability and convergence, it is observed how appears a finite detuning for high spectral components, causing the characteristic dispersive oscillations. On the other hand, the finite difference method used always introduces some amount of artificial dispersion that modify the dispersion relations. However, the oscillatory solutions, e.g. Fig. 2.16, are therefore not caused directly by numerical artifacts. They are not present in homogeneous simulations. Note the grid used is 300 elements per wavelength and the artificial attenuation was only 10^{-3} P/s, ten times greater than the water viscosity. The effect of computational restrictions is to slightly modify the dispersion relations for higher harmonics causing finite detuning. We expect those effects to be present in real materials, and therefore, limit the ability of recovering perfect coherence for all spectral components and create shock waves[3].

Other interest feature is that in these conditions phase speed at the fundamental and at higher harmonic frequencies always match $c_p(n\omega) = \bar{c}_0$. In contrast, in this situation the group velocity does not match necessary the low frequency sound speed. In this case was close, with a value of $c_g = 0.97\bar{c}_0$.

Other situations can be explored by changing the layered parameters. Figure 2.17 (top)shows the dispersion relation for $c_1/c_2 = 2$ and $\alpha = 0.1$. It is shown in Fig. 2.17 (bottom) that coherence is achieved, at least for the lowest components, for $\omega/\Omega = 1.22$. In this case, the phase speed matches $c_p(n\omega_0) = \bar{c}_0$, but the group velocity is reduced to $c_g(\omega_0) = 0.830$. Figure 2.18 shows the evolution of the fundamental and its first two harmonics. A remarkable effect that can be observed here is the appearance of high-amplitude oscillatory fields due to the strong impedance contrast between layers, actually nonlinear Bloch waves. In these reduced group velocity conditions, the analytical solution for homogeneous media (dashed lines) does not match the numerical results. However, no beating are produced and the shape of harmonic growing is essentially the same. It can be seen that the rate of second and third harmonic growth is increased. The distance at

[3]Other interesting topic, not studied here, is to find conditions for recovering coherence in media with attenuation by tuning its lossy dispersion relations

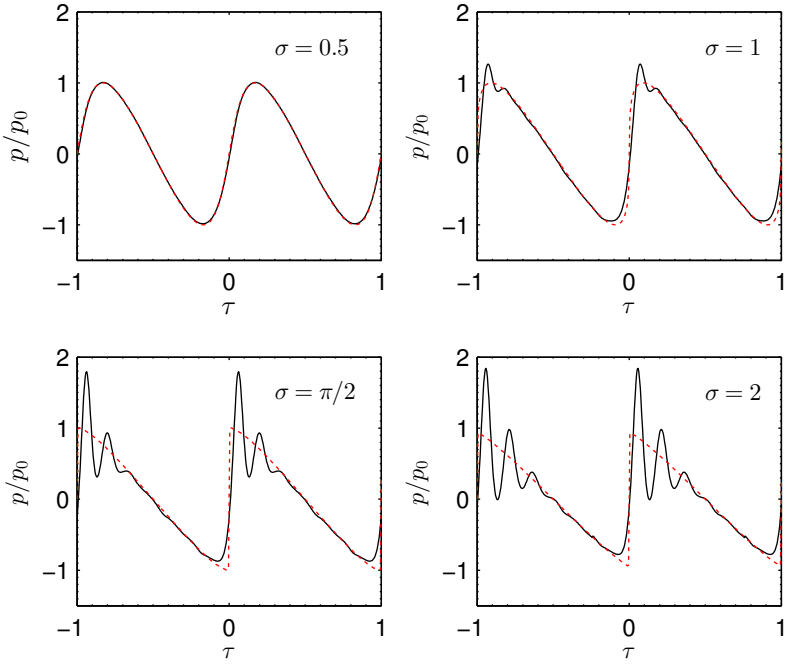


Figure 2.16: (continuous lines) Waveforms at different distances ($\sigma = 0.5, 1, \pi/2, 2$) for $\omega_0 = 1.75/\Omega$ where a coherence is recovered for the lowest harmonics. Blackstock analytic solution (red dotted lines).

which the maximum second harmonic field is produced is located at $\sigma \approx 1.2$ in the homogeneous media while in the numerical simulations appears at $\sigma = 0.7$. Same scaling is observed for the rate of harmonic generation, where in the homogeneous media (near the source) second harmonic grows at a rate $p_0\sigma/2$ Pa/σ, and in the numerical simulations the rate of growing was $0.86p_0/\sigma$ Pa/σ. The whole effect is that the effective nonlinearity of the system in these conditions is increased. For the present case, a factor of increased nonlinearity can be obtained by fitting the analytical solution to the numerical results, letting as the free variable an effective parameter o nonlinearity, namely $\bar{\beta}$. Thus, for the presented results, a factor of $\bar{\beta} = 1.72$ is estimated. A new solution using this effective parameter is shown in Fig. 2.17 (bottom) in thick lines. It can be observed how the fitted solution agrees the slow-group speed for distances up to the effective shock distance (0.58σ in the figure). The observed effect of retaining coherence and reduce group velocity is to increased the effective nonlinearity of the media together with the apparition of high-amplitude nonlinear Bloch waves.

In the following subsections, we propose and analyze different interest layered

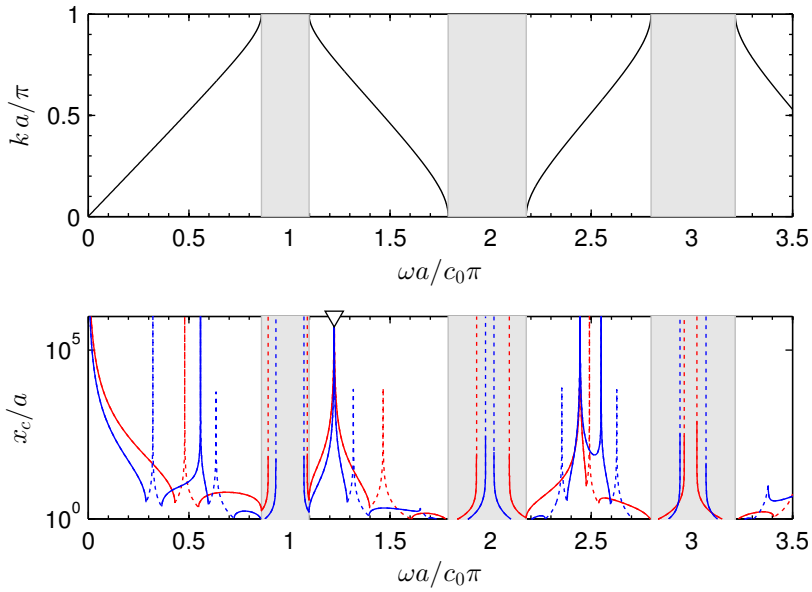


Figure 2.17: (Top) dispersion relation for a layered media of $c_1/c_2 = 2$ and $\alpha = 0.1$. (Bottom) coherence length for second (red) and third (blue) harmonic in function of the fundamental frequency. Frequencies at which the fundamental frequency is in band-gap are is marked in gray regions, while band-gap regions for second and third harmonic are marked in dashed lines.

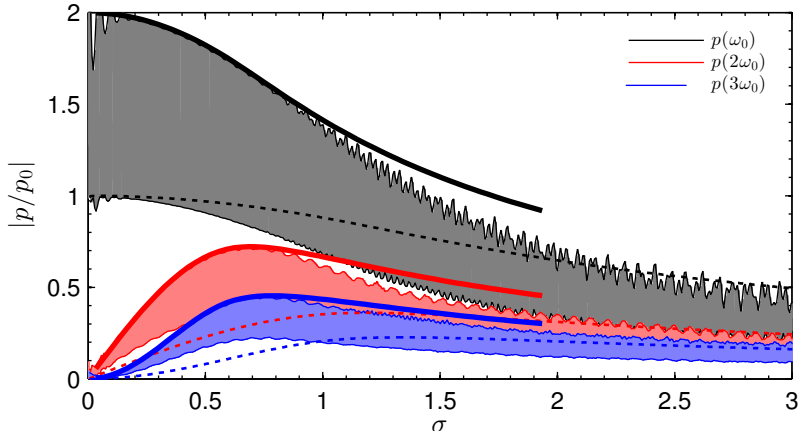


Figure 2.18: Harmonic distribution for the frequency $\omega_0 = 1.22/\Omega$. Blackstock solution (dotted lines).

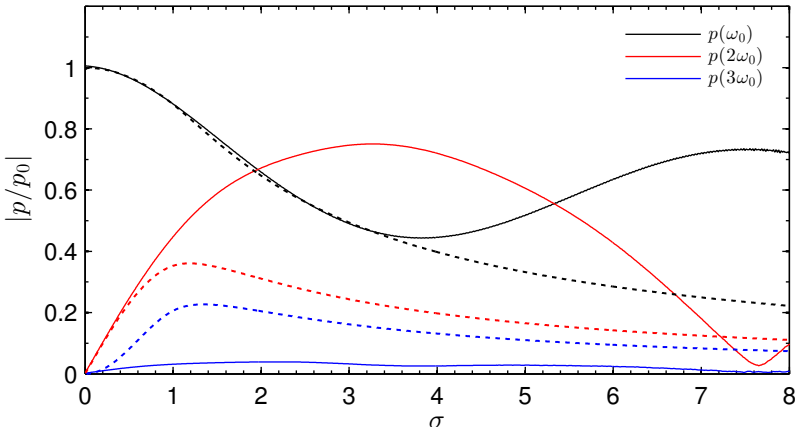


Figure 2.19: Harmonic distribution for $\omega_0 = 1.668/\Omega$ where a coherence is achieved for second harmonic while the frequency of the third harmonic falls into the bad-gap.

media designs with specific balance between between detuning, evanescent propagation and synchronous generation.

2.5.2 Increasing second harmonic generation

One can expect that second harmonic generation is maximized in homogeneous nondispersive media. However, in nondispersive media coherence is achieved not only at second harmonic frequency, but also in the higher spectral components. As a result, energy is transferred from second harmonic field to higher spectral components and therefore second harmonic field does not grow indefinitely. Moreover, shock waves are formed and nonlinear absorption reduces wave intensity for $\sigma > \pi/2$ even in lossless media (Hamilton et al., 1998a).

The controlled dispersion of the layered system can modify this situation by including dispersion that alters the higher harmonic cascade processes while maintaining coherence for second harmonic. Figure 2.14 shows an example of a dispersion relation where for $\omega_0 = 1.668/\Omega$ it can be observed that there exist a reasonable coherence for the second harmonic ($x_c/a \approx 1000$ lattice units), while the third harmonic falls in a band-gap. Figure 2.19 shows the harmonic distribution in this situation. Here, energy is transferred to second harmonic field that grows almost linearly for $\sigma < 2$. On the other hand, the energy transferred from second to third harmonic is not cumulative and its amplitude does not grow with distance. Third harmonic experiment evanescent propagation due to the imaginary part of the complex wave-vector at this frequency. A constant field, as studied in Sec. 2.4.4, is obtained for the third harmonic.

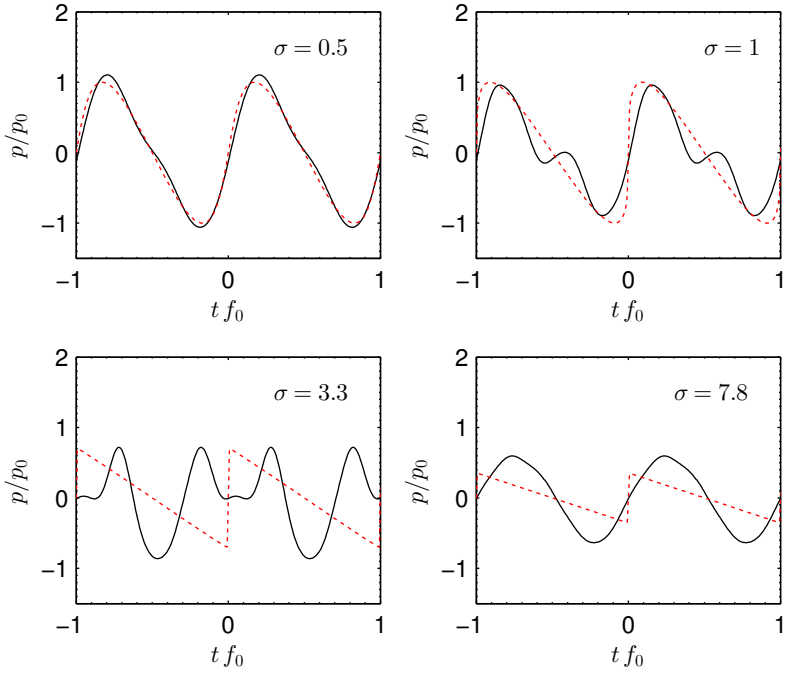


Figure 2.20: (continuous lines) Waveforms at different distances for $\omega_0 = 1.668/\Omega$. At $\sigma = 3.3$ second harmonic generation field is maximize and can be seen the period doubling in the waveform. Then, at $\sigma = 7.8$ due to second harmonic detuning nearly sinusoidal wave is recovered. Blackstock analytic solution (red dotted lines).

The total amount of the second harmonic amplitude in nondispersive media is $p_2|_{\max} \approx 0.36 p_0$, while in the example of Fig. 2.19 a maximum second harmonic amplitude of $p_2|_{\max} \approx 0.75 p_0$ is predicted. As can be shown the decreasing of the first harmonic follows the analytic nondispersive Blackstock solution for $\sigma \lessapprox 3$. Thus, in this regime all the energy of the first harmonic is being transferred to the second harmonic field. However, due to finite detuning of the second harmonic a long spatial beating is produced, with period 8σ, and energy is returned back to the first harmonic component.

It is worth noting here that at distance $\sigma \approx 3$ sawtooth profile is observed in nondispersive media. In contrast, only second and first harmonic have remarkable amplitude into the layered media. Waveforms are shown in Fig. 2.20. Near the source, where the amplitude of higher harmonics in not relevant the nondispersive waveform (in red dotted) is well approximated by the fundamental and its second harmonic of the layered medium. However, due to the evanescent propagation of the third harmonic for longer distances the nonlinear solution of the layered medium is mainly composed by the fundamental and its second harmonic. The

maximum second harmonic in this configuration is observed at $\sigma = 3.3$, where it can be appreciated in the waveforms of Fig. 2.20 the period doubling. Moreover, due to finite detuning of the second harmonic the process is not cumulative for all distances and at $\sigma = 7.8$ the energy is restored in the first harmonic again and a sinusoidal wave is obtained[4]. An analogous effect has been also studied (Naugolnykh et al., 1998) where instead of dispersion, selective absorption at specific frequencies is used to modify and enhance harmonic generation.

2.5.3 Increasing third harmonic generation

In the first band ($\omega < \Omega_0$), coherence is always lower for the third harmonic than for the second. However, in the superior bands the layered medium parameters can be tuned to obtain higher coherence for the third than for the second harmonic. Essentially we follow same ideas on the preceding section but for the third harmonic. In this case, the lattice is designed forcing the second harmonic to fall in bandgap. A the same time, perfect coherence can be found for the third harmonic at $\omega = 0.529\Omega_0$. This situation is illustrated on Fig. 2.21. In this case, the dispersion relation was obtained for a layered medium with parameters $\alpha = 0.3$ and $c_2/c_1 = 1/3$.

In this situation, as Fig.2.22 shows, second harmonic field present a constant value of about $0.04p_0$. As discussed in Sec.2.4.4, this constant field does not grow with distance and is related to the evanescent solution of the *free* wave and the local nonlinear "pumping". On the other hand, due to the coherence of the third harmonic, all the energy transferred form second to third is accumulated with distance. Therefore, near the source the rate of energy transfer from second to third harmonic is constant. Thus, third harmonic start to grow almost linearly with distance, opposite to quadratically in homogeneous media.

Also it can be seen in the simulations how fourth and fifth harmonics grow (red dotted and blue dotted lines in Fig. 2.22). In this case only fifth harmonic have remarkable amplitude, growing near the source almost quadratically with distance. Therefore, the entire system behaves as an artificially cubic-like nonlinear medium formed by quadratic nonlinear layers.

The corresponding waveforms measured at $\sigma = (0.5, 2, 8, 12)$ are shown in Fig. 2.23. For $\sigma = 0.5$ and 2, it can be observed how the wave steepens with the characteristic shape of cubic nonlinearity. No shock waves are formed as long strong dispersion is present for high frequency harmonics. However, it is worth noting here a remarkable fact: it steepens in the positive time axis direction (to

[4]Note all the energy is not restored to first harmonic in Fig. 2.19 at $\sigma = 7.8$, leading to a sinusoidal wave of different amplitude as can be observed in Fig. 2.20. The energy loss is mainly due to the artificial (numerical) viscosity necessary to nonlinear convergence(Hamilton et al., 1998a). For these simulations the total distance is 1200 lattice sites and therefore the effects of attenuation are not negligible. However, the main nonlinear effects related to strong lattice dispersion still appreciated.

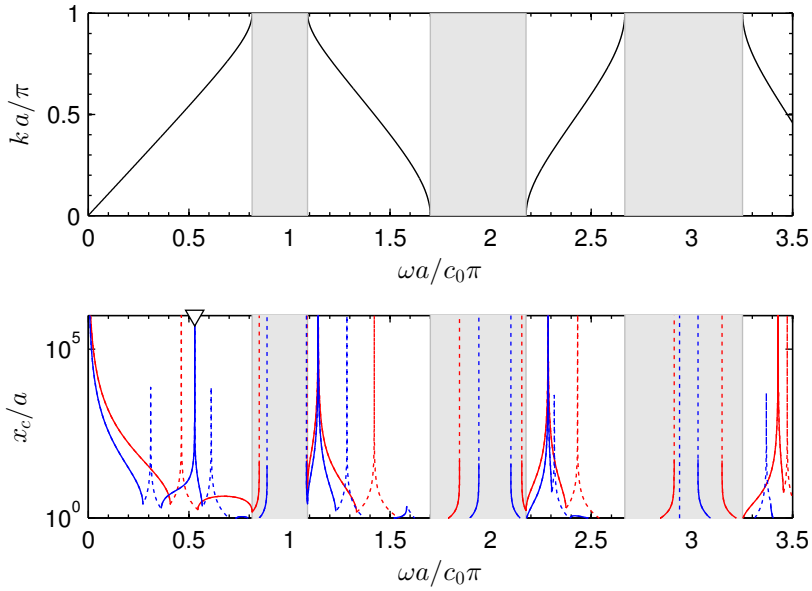


Figure 2.21: Harmonic distribution for $\omega_0 = 1.668/\Omega$ where a coherence is achieved for second harmonic while the frequency of the third harmonic falls into the bad-gap.

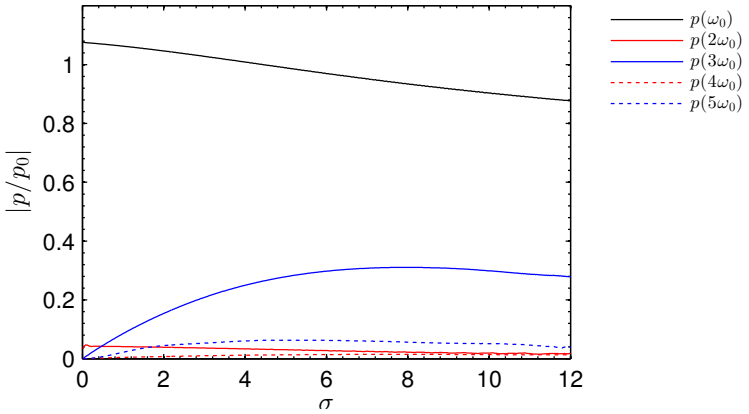


Figure 2.22: Harmonic distribution for $\omega_0 = 1.668/\Omega$ where a coherence is achieved for second harmonic while the frequency of the third harmonic falls into the bad-gap.

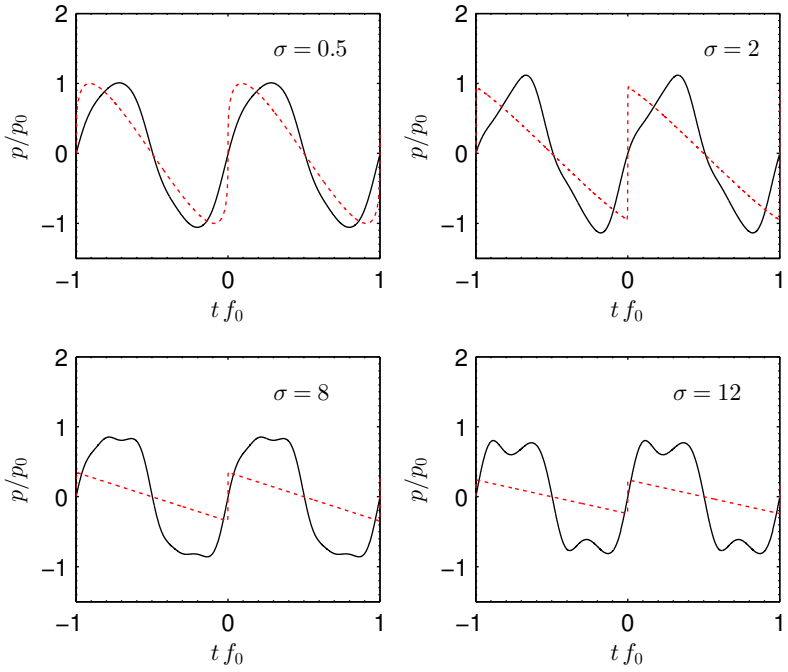


Figure 2.23: (continuous lines) Waveforms at different distances for $\omega_0 = 1.668/\Omega$. At $\sigma = 3.3$ second harmonic generation field is maximize and can be seen the period doubling in the waveform. Then, at $\sigma = 7.8$ due to second harmonic detuning nearly sinusoidal wave is recovered. Blackstock analytic solution (red dotted lines).

the right in the figure), opposite than the quadratic nonlinearity plotted in red dotted as a reference. This effect, i.e. the steepening on the opposite side of the propagation direction, is characteristic of materials with negative parameter of nonlinearity. Therefore, the effective nonlinear behavior observed by the simulations in this conditions can be described as negative-cubic-like nonlinearity.

2.5.4 Acoustic *Fluorescence* in chirped layered media

Another interesting configurations can be achieved by adiabatically changing the lattice period, $a = a(\mathbf{x})$, of the layered medium, namely chirped layered media. Analogues to these configurations, chirped periodic media has been studied in linear regime in optics (Cheng et al., 2014) or in acoustics using arrays of distributed cylindrical scatterers (Romero-García et al., 2013). Using these chirped configurations band-gap can be placed at different locations for different frequencies. Here, we design a system with increasing lattice period, where the band-gap for

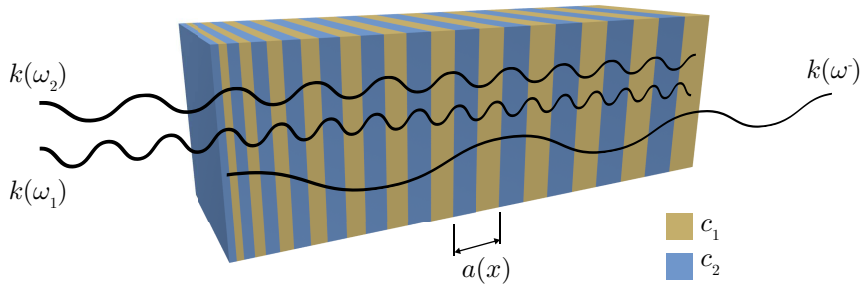


Figure 2.24: Scheme of the acoustic "fluorescence" effect. The chirped system is radiated with two waves of slightly different fundamental frequencies ω_1 and ω_2. Harmonics are generated at combination frequencies inside the medium and at the end of the system the period is tuned to achieve a band-gap at fundamental frequency. Thus, only the low-frequency difference-component is transmitted.

the fundamental component of two nearly similar frequency waves is located at the end of the chirped layered medium. Thus, as sketched in Fig. 2.24, two harmonic waves with close frequencies are injected at the beginning of the lattice. In this region, the lattice period is designed small enough to achieve good coherence so harmonics at combination frequencies can be generated progressively through the layered system. Then, at the end of the lattice the period is decreased in such a way that it correspond to a forbidden band for the fundamental component.

In this case, the frequency of the waves was selected to be $f_1 = f_0$ and $f_2 = f_0 + f_0/3$. Figure 2.25 (top) shows the bandgap location in the lattice, that is located at $x = 0$ until $x = 200a$. Then, the rest of the domain is homogeneous. Although it is calculated for infinitely period media, we assume that the band gap exist for the adiabatic chirped lattice. Figure 2.25 (bottom) shows the harmonic evolution for this configuration where it can be seen how harmonics at combination frequencies are generated at the beginning of the lattice. The bandgaps of layered medium act as spatial filtering for the fundamental components that are reflected back around $x/a = 100$, leading to an enhancement of the field discussed in (Romero-García et al., 2013). This enhancement is clearly visible in Fig.2.25 (bottom). Furthermore, not only fundamental frequency is filtered. As long the bandgap central frequency change with distance, the superior bandgaps cover the entire frequency range, reflecting back higher harmonics.

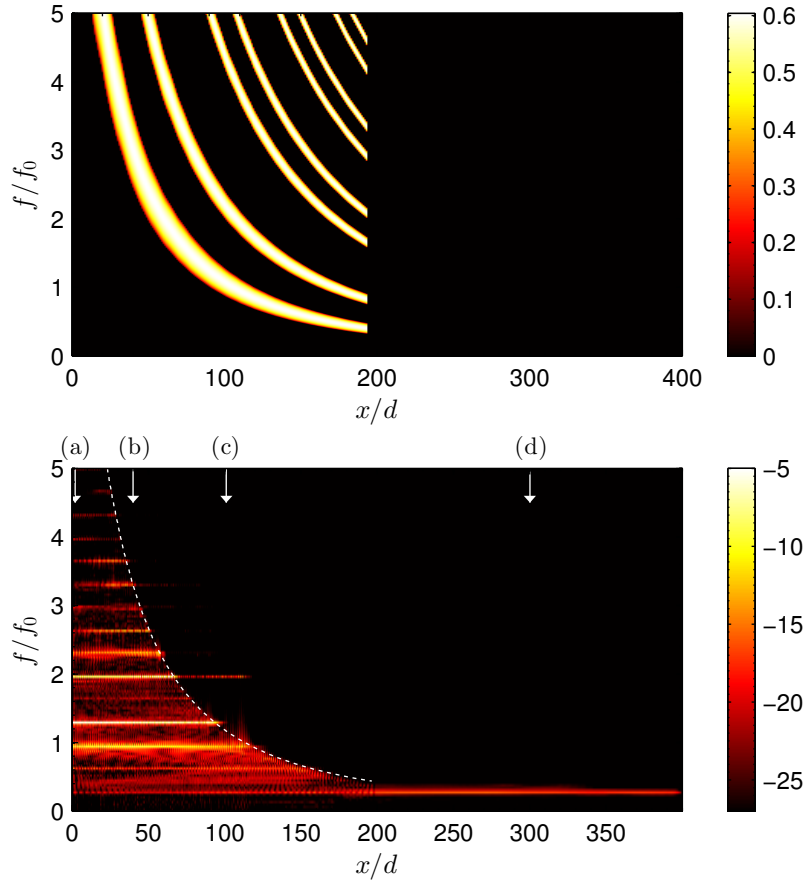


Figure 2.25: (top) Bandgap distribution in function of space. The chirped lattice ranges from $x = 0$ to $x/a = 200$, (middle) Spectrum-spatial distribution, (bottom) harmonic distribution for fundamental waves, its second harmonics and the difference component.

Therefore, only the difference frequency wave can be transmitted trough the medium. The final effect is that in transmission an effective demodulation is achieved: an amplitude modulated wave is injected, see Fig. 2.26 (a), the difference frequency is nonlinearly generated among other combination frequencies Fig. 2.26 (b-c), and the system output is only the low frequency component.

The whole effect presents some analogy with fluorescence, where electrons re-emit a photon when relaxing to a lower quantum state after being exited with some electromagnetic wave. The emitted light has, in most cases, a longer wavelength and lower energy, than the absorbed radiation. Obviously, this analogy is not formal and only conceptual.

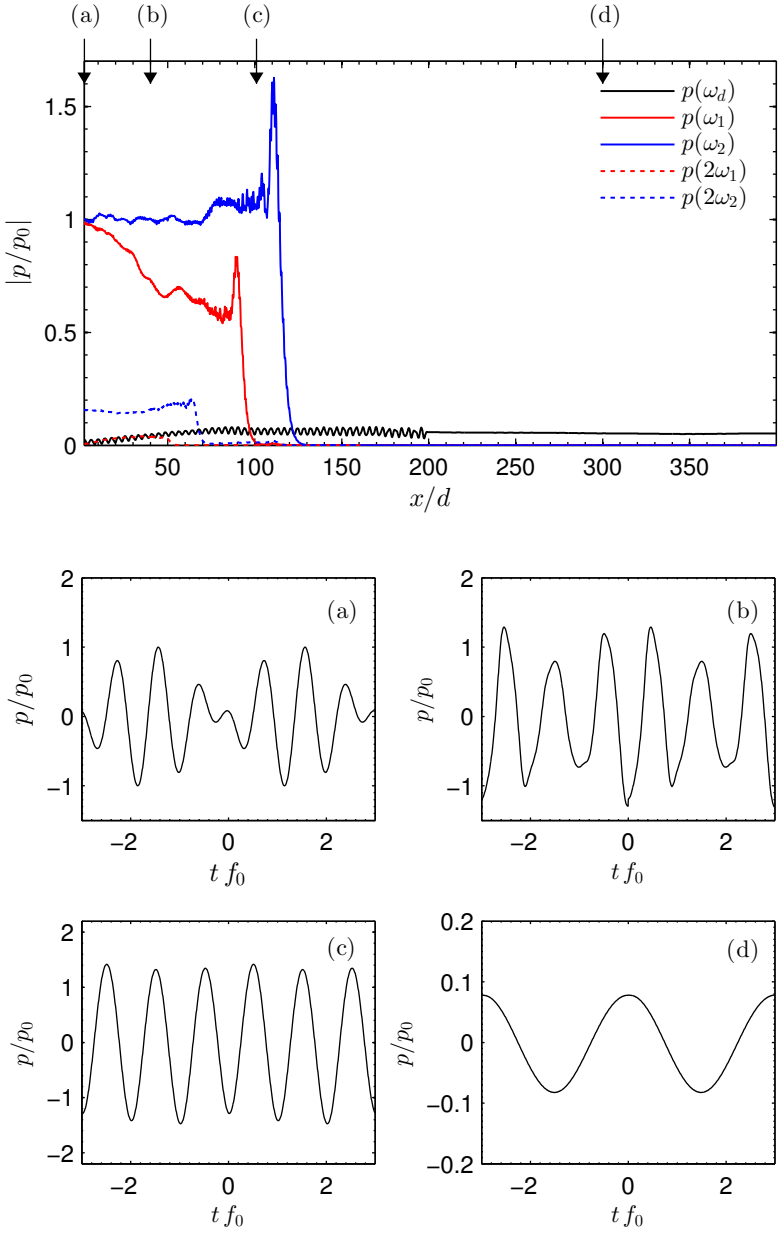


Figure 2.26: (Top) Harmonic distribution in the chirped layered media where the acoustic "fluorescence" is observed. The self-demodulation of the two collinear modes is achieved inside the nonlinear media, while the band-gap at the end of the chirped layered media limits the transmission of the high frequency components. Therefore, only the self-demodulated component is transmitted. (Bottom) Corresponding waveforms observed at locations (a-d).

2.5.5 Frequency Conversion Mirror in chirped layered media

We propose a setup of the chirped layered media in which the bandgap is located for the frequency of the second harmonic at the end of the structure. Actually, the structure is equivalent to the preceding subsection, but a monochromatic fundamental wave is selected here at frequency ω^{-}. The fundamental wave is therefore a propagating mode over all the structure. On the other hand, its second harmonic only can propagate trough the beginning part of the structure. At the end of the layered media, its corresponding wavevector presents an imaginary part and the propagation is evanescent. Therefore, it is reflected back to the source. From the point of view of the source, the whole process can be treated as a nonlinear mirror: the incident wave is reflected with doubled frequency.

In order to visually illustrate the process, simulations were carried out using a k-space method over a 2D domain. The incident wave was generated by a Gaussian beam at frequency ω, steered 10^{o} from the axis of the structure, see Fig. 2.27. It is worth noting here that the theoretical dispersion relation is one-dimensional and for non-normal incidence angles it will change. However, for illustrate the processes and for the selected incident angles is enough.

Figure 2.28 shows the first and second harmonic field, with the structure in the middle and the source below. It can be seen that when the intense wave impact on the layered, its first harmonic is slightly refracted due to different phase speed in the outside media and in the layered structure. Then, it shows very high transmission out of the structure. Only spurious reflection of the first harmonic is observed due to the impedance mismatching at the boundaries of the structure: in both limits of the crystal (top and bottom) reflection can be observed. On the other hand, the second harmonic is generated at the beginning of the propagation and inside the structure. The transmission of second harmonic is negligible. It can be seen how its amplitude becomes negligible in the bandgap area marked by

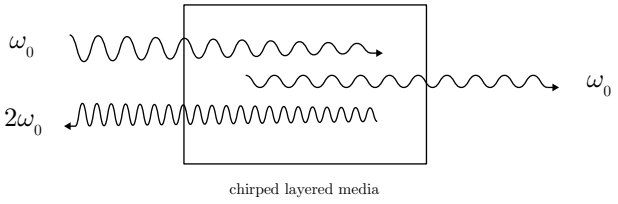


Figure 2.27: Scheme of the *frequency conversion mirror* effect. A wave with fundamental frequency ω_0 enters in the chirped system. Second harmonic is generated inside the medium and at the end of the system the period is tuned to achieve a band-gap at second harmonic frequency. Thus, second harmonic is reflected while fundamental field is transmitted.

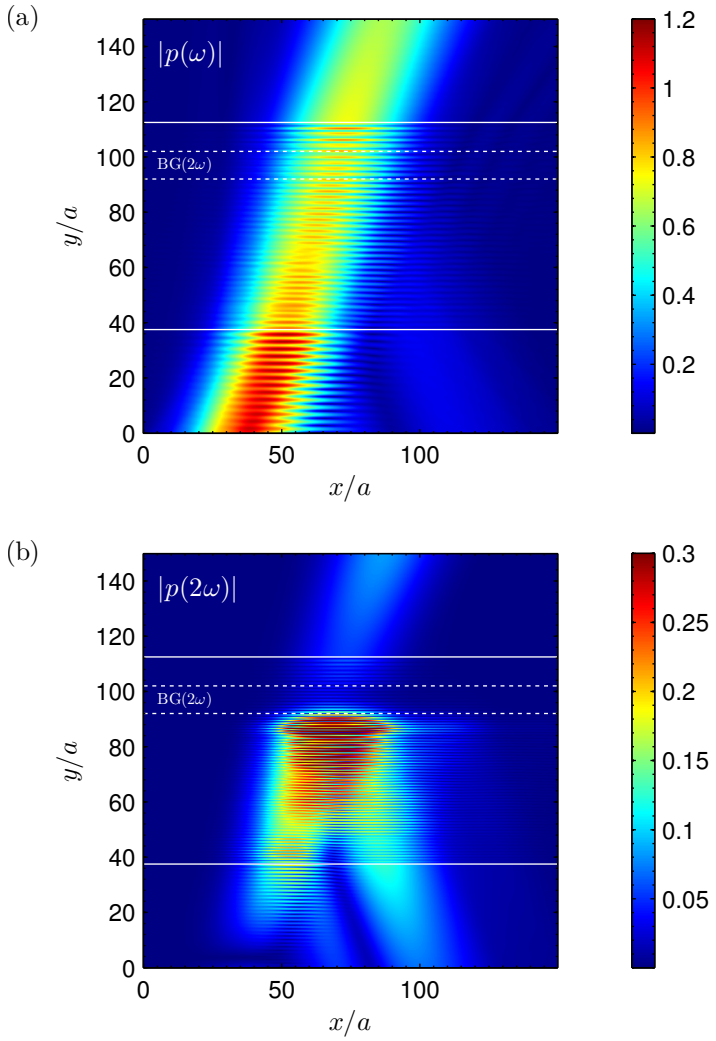


Figure 2.28: Field distribution for (a) first harmonic and (b) second harmonic field in the frequency conversion mirror configuration. The chirped layered media extends between white lines. White dotted lines marks the extension of the bandgap for the second harmonic.

the dotted lines. After the end of the gap, first harmonic start again generate harmonics by cascade processes, and second harmonic field increases, but the second harmonic generated at the beginning is not transmitted. The energy that is not transmitted is reflected back, as can be seen in Fig. 2.28 (b). In addition, reflection at the bottom boundary can be also observed due to impedance mismatching.

The effects of the present configuration can be enhanced by using very high

nonlinear material in the construction of the layered media than in the surrounding fluid. Thus, for instance using layers of bubbly fluids and solid plates with micro cracks the nonlinear generation of second harmonic can be located only inside the layered structure and if the bandgap is properly designed at the end of the lattice the transmission of second harmonic will be negligible. On the other hand, controlling the length of the crystal and the steering of the beam the reflection of the second harmonic can be uncoupled totally from the reflections of the first harmonic field. Another improvements include focalization of the reflected harmonics as achieved in optics for linear waves (Cheng et al., 2014).

2.5.6 β-Modulated media

Finally, instead of modulate the sound speed and density of the layers, the nonlinear parameter of the media can be also modulated. Thus, it is interesting to take into account that there exist some materials, most of them solid, that exhibit negative nonlinearity. These materials are well-known and also common, e.g. some glasses as Pyrex or fused silica (Hamilton et al., 1998a). The nonlinear processes in negative nonlinear parameter media are not completely different from the positive ones. The nonlinear parameter shows the dependence of sound speed on pressure. Thus, the difference between positive and negative nonlinear media is that in negative media the rarefaction cycles of the wave travels faster than the compression cycles. Thus, wave profile distortion, as Fig. 2.29 sketches, is simply inverted.

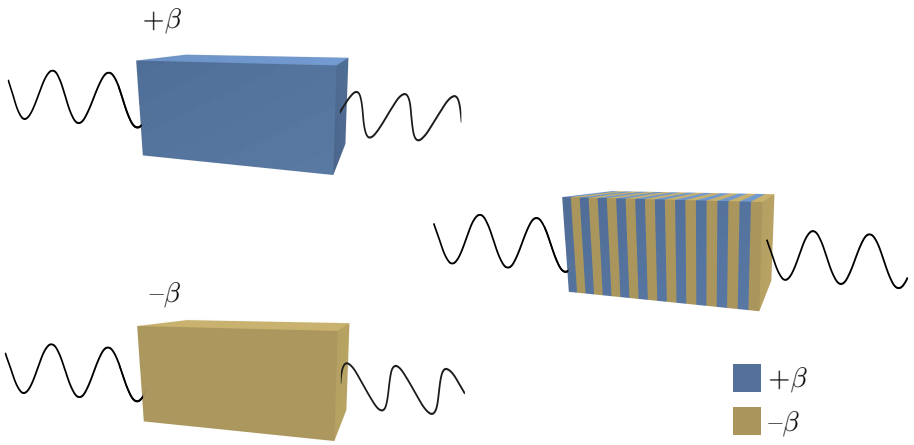


Figure 2.29: Scheme of the β-modulated acoustic layered media. (top-left) The nonlinear distortion in an homogeneous layer with $+\beta$ leads to steepening in the $+z$ direction, while for $-\beta$ the steepening is produced in the opposite direction. Therefore, alternating thin layers of positive and negative nonlinearity the steepening distortion can be mitigated.

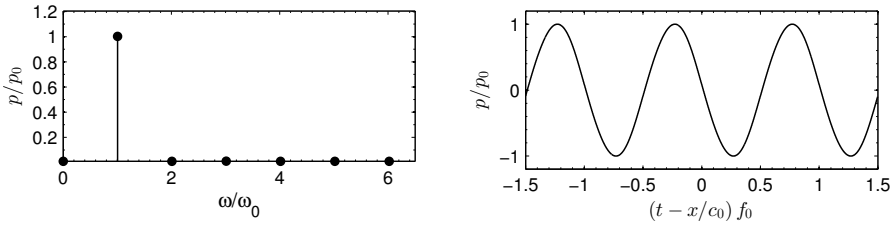


Figure 2.30: (Left) Spectrum obtained at $\sigma = 1$ for a wave traveling a the β-modulated material. (Right) Corresponding waveform.

Then, we propose a configuration where thin layers of two materials with inverted nonlinear parameter are alternated. The idea is that the distortion during propagation in one layer is compensated by the distortion in the following and thus, a extremely linear material can be generated for supporting very intense waves at distance much longer than the shock formation distance. For the sake of simplify, the density and sound speed will be maintained equal in both media. The layer thickness was set to $a = 0.1\lambda$ and the nonlinear parameters as $\beta_1 = -\beta_2 = 5$, of the order of the common materials.

Extremely linear media

Figure 2.30 shows the waveform and its spectrum recorded at the shock distance. It can be observed the absence of nonlinear distortion. due to the negligible energy transference to higher harmonics the fundamental component retains its initial amplitude. The evolution of the spectral components versus distance is shown in Fig. 2.31. It can be observed that the monochromatic wave can travel at the shock distance without experiment distortion.

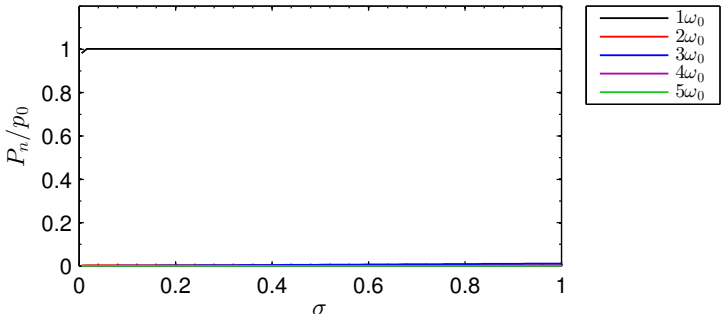


Figure 2.31: Harmonic evolution in the β-modulated material. Up to the shock wave distance almost all the energy remains in the fundamental harmonic and the harmonic amplitude for the higher spectral components is negligible.

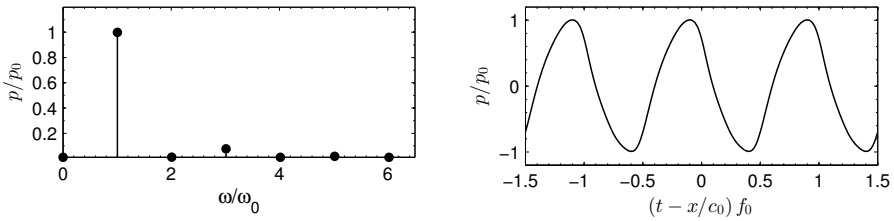


Figure 2.32: (Left) Spectrum obtained at $\sigma = 10$ for a wave traveling a the β-modulated material. (Right) Corresponding waveform.

Cubic nonlinear composite media

However, an interesting effect is also observed. If the propagation is long enough, some harmonics of the fundamental frequency appears, but only the odd harmonics are generated. Thus, response of the media appears to be effectively equivalent to a cubic media. An explanation of this phenomena can be obtained for nondispersive propagation. The asymptotic expressions for the amplitude of the harmonics near the source can be obtained by expanding the Bessel-Fubini Eq (2.37). The expansion leads to the expressions for the second and third harmonics:

$$p_2(x,\tau) = \frac{\beta p_0^2 \omega}{2\rho_0 c_0^3} x \sin 2\omega\tau, \tag{2.53}$$

$$p_3(x,\tau) = \frac{3\beta^2 p_0^3 \omega^2}{8\rho_0^2 c_0^5} x^2 \sin 3\omega\tau. \tag{2.54}$$

It can be seen that the second harmonic grows linearly with the distance and it is proportional to the nonlinear parameter β. On the other hand, the third harmonic depends quadratically on both variables. Then, if a wave travels trough a layer of the proposed structure with $\beta_1 = +\beta$, its second harmonic will increase

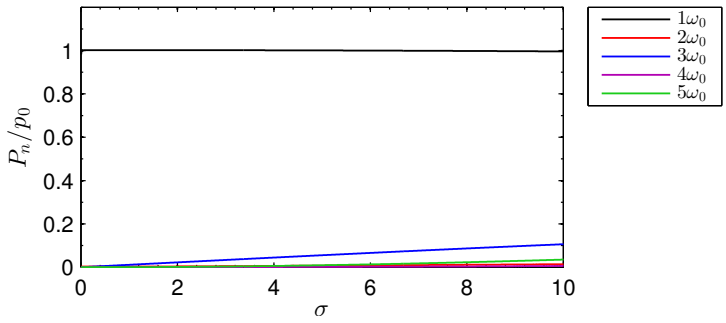


Figure 2.33: Harmonic evolution in the β-modulated material, where it can be seen the generation of odd harmonics.

linearly and the third, almost absent, will do quadratically. When the wave crosses the next layer with inverted nonlinearity $\beta_2 = -\beta$, Eq. 2.53 contributes creating the same amount of second harmonic than in the preceding layer but inverted due to the $-\beta$ coefficient, i.e. with opposite phase. Therefore, second harmonic at the end of the second layer vanishes. This process holds for thin layers were the asymptotic expressions can be applied. However, the generation of third harmonic depends on β^2, so there does not exist cancellation between layers and the generation is cumulative with distance. Third harmonic is generated by cascade processes and needs second harmonic field. Due to second harmonic is generated and compensated periodically, the evolution of the third does not grows quadratically with distance and its rate of the generation is very slow.

Figure 2.33 presents the evolution of the spectral components for distances up to $x = 10x_s$. It can be observed that the odd harmonics are generated and the even ones vanishes. On the other hand, the generated third harmonic shows an almost linear dependence with propagation distance, where the fifth harmonics grows at a quadratic rate. Figure 2.32 shows a waveform recorded at $\sigma = 10$, where the characteristic shape of cubic nonlinearity can be observed, see e.g. (Jacob et al., 2007). On the right plot, its spectrum revels an almost negligible contribution of the even harmonics.

The configuration proposed, opens a way to obtain cubic nonlinearity for the longitudinal waves from a layered distribution of quadratic nonlinear materials. Therefore, such structure can be designed also using solid composites in the micro scale to obtain new ways of management of acoustic waves as low distortion waveguides for intense perturbations where the acoustical saturation distance can be extended. In the more general case including dispersion, the system offers the possibility of designing new tunable nonlinear materials where phase velocity and effective nonlinearity can be modified to achieve exotic configurations, while the structure is made from common material composites.

2.6 Dispersion managed acoustic solitons

One of the most widely studied phenomena in most nonlinear and strongly dispersive media is the existence of solitons. Solitons are nonlinear localized perturbations that propagate without changing its shape, emerging from the interaction of nonlinearity and dispersion. The first observation of the solitary waves was in 1834 by John Scott Russell at the Union Canal in Scotland, who called them *Waves of Translation*. In its experiments Russel described the main properties of these shallow-water waves (Russell, 1844). Starting from the theoretical works of Boussinesq and Rayleigh (Boussinesq, 1871; Boussinesq, 1877; Rayleigh, 1876), these waves could not been completely explained by the existent theory of water waves until 1895 when the Diederik Korteweg and Gustav de Vries derived a simple partial differential equation for shallow-water waves (Kordeweg et al., 1895).

Their model, now known as the KdV equation, is completely integrable and provides exact solutions as solitons and cnoidal waves. However, it was not widely studied until 1965 with the advent of the computational physics when Zabusky and Kruskal found that the KdV model arises as the continuum limit of the FPU nonlinear lattice (Zabusky et al., 1965).

From these seminal works, solitary-wave solutions have been observed and deeply studied in most physical systems that can support nonlinear and dispersive waves: electromagnetism and nonlinear optics; hydrodynamics; acoustics, elastodynamics and granular media; phononics and nonlinear molecular dynamics, DNA dynamics, Bose-Einstein condensates, plasmas and so on. The solutions presented Chapter 1, in the limit of weak dispersion and weak nonlinearity, can also be described by the KdV equation. The acoustic layered media is not an exception.

Solitons have been studied by Yong et al. (2003) in layered acoustic media and in also in media with alternated solid and fluid layers (Fainstein et al., 2013; Huynh et al., 2015). Here, we extend the analysis using numerical techniques in the limits of strong nonlinearity and strong dispersion, i.e. from the long and slow solitons to sharp and intense acoustic solitary-waves.

2.6.1 KdV solitons

The Korteweg-de-Vries (KdV) equation arises as the continuum limit of the FPU quadratic nonlinear lattice (Zabusky et al., 1965). Thus, in the low frequency limit both models can be described by the same dispersion relation. Consider the dispersion relation of a mono-atomic lattice as

$$\omega^2 = \omega_M^2 \sin\left(\frac{ka}{2}\right)^2, \tag{2.55}$$

where c_0 is the small amplitude sound speed and a the oscillator separation, and the upper cut frequency is $\omega_M = 2c_0/a$. We can expand in Taylor series this lattice dispersion relation around $k = 0$, retaining up to cubic terms leads to the KdV dispersion relation:

$$\omega(k) = c_0 k - bk^3, \tag{2.56}$$

with

$$b = \frac{1}{24} c_0 a^2 \tag{2.57}$$

as the dispersion parameter of the low frequency limit for longitudinal vibrations in any mono-atomic lattice. Figure 2.34 shows the normalized dispersion relation for the lattice and its KdV low frequency approximation, where it can be appreciated

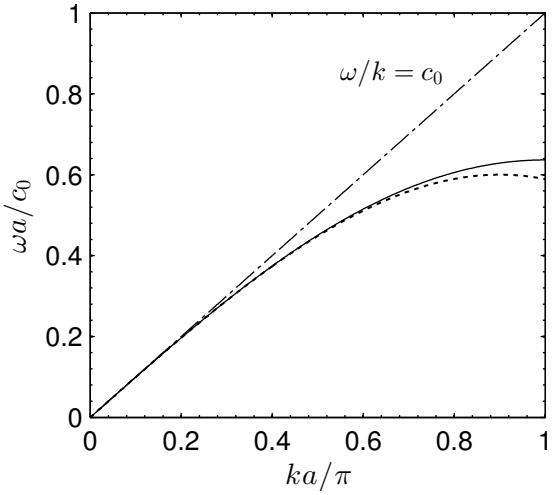


Figure 2.34: Dispersion relation for the mono-atomic lattice (continuous) and its KdV low frequency regime (dotted). Nondispersive slope is plotted in dashed-dotted line for comparison.

that both models fit very well for long wavelengths, but also for remarkable high wavenumbers. Relative difference is below 1% for wavenumbers below $kd/\pi < 0.64$. However, the group velocity in this equivalent KdV is lower then in the full lattice, and it decreases faster with frequency.

Seen that similarity between band structures, and given the fact of the same quadratic nonlinearity is present in the KdV model and the FPU lattice, it is not surprising that similar solutions can be obtained in both systems, at least in the low frequency regime. The solutions explored in the Coulomb chain presented in Chapter 1 can be obtained also by the KdV equation provided that the kinks are far of the ultra–discrete regime, e.g. for energies below 0.5 eV.

Furthermore, homogenization techniques can applied to the layered media (Santosa et al., 1991), where, despite the complexity of the superior bands, the dispersion relation in the first band present the same shape under some assumptions than the FPU lattice. Therefore, a Taylor series expansion of Eq. (2.1) in powers of ω around $\omega = 0$, collecting terms up to second order, leads to

$$\omega^2 \approx (1 - \cos(ka)) \frac{2c_1^2 c_2^2}{a\,(a_2 c_1^2 + a_1 c_2^2)}\,. \tag{2.58}$$

Then, we expand again in Taylor series in powers of k around $k = 0$, and collecting terms up to third order we get

$$\omega \approx \sqrt{\frac{ac_1^2c_2^2}{a_2c_1^2+a_1c_2^2}}\,k - \frac{a^2}{24}\sqrt{\frac{ac_1^2c_2^2}{a_2c_1^2+a_1c_2^2}}k^3\,, \tag{2.59}$$

that can be expressed in the compact KdV form

$$\omega(k) = c_0k - bk^3\,, \tag{2.60}$$

with the parameters

$$c_0 = \sqrt{\frac{ac_1^2c_2^2}{a_2c_1^2+a_1c_2^2}} \tag{2.61}$$

$$b = \frac{a^2}{24}c_0\,. \tag{2.62}$$

Note the dispersion parameter is exactly the same that obtained for the FPU mono-atomic lattice.

However, this result only states that both models are similar around $k = 0$, but there can exist remarkable differences between the layered system and its equivalent KdV model for short waves when $ka \to 1$. Figure 2.35 shows the full dispersion relation for three different α ratios and its asymptotic solution for the low frequency regime by Eq. (2.60). It is clearly seen that good agreement between the mono-atomic lattice and its KdV expansion is only achieved in the case of $\alpha = 0.9$ and $c_2/c_1 = 0.1$. For the other cases ($\alpha = 0.1$ and $\alpha = 0.5$), the first propagation band becomes flatten, the frequency at which the band-gap start becomes higher and therefore the band-gap stretches. In the limit of Eq.(2.1) for $\alpha \to 1$ and $c_2/c_1 \to 0$, the first band of the layered matches exactly the mono-atomic chain dispersion relation Eq. (2.55), while the second band does not start in a finite frequency, i.e. there does not exist superior bands. This limit shows that the first band most dispersive shape for the layered medium is the dispersion relation Eq. (2.55). This situation corresponds to the case of a homogeneous media with infinitesimal-sized soft inclusions. Note that the inclusions impedance contrast must be large and also that the sound speed of the inclusions must be is low than the host media. A good analogy of this situation, for small amplitude waves[5], is a one dimensional version of a liquid with period inclusions of gas bubbles. Also note in one dimensional system a rigid inclusion ($c_2/c_1 = 0$) implies zero transmission and therefore no wave inside the structure, increasing c_2/c_1 to low but physical values mean strong dispersion.

On the other hand, the effect of the layered medium dispersion is to *flatten* the slope of the first propagation band for high spatial frequencies, from the critical

[5]Soft inclusion typically shows large compressibility values and for finite amplitude waves the inclusions, in this case bubbles, are large compressed. Therefore, large strains are produced and the material response is described not only by its compressibility, but a large fraction of its local nonlinearity.

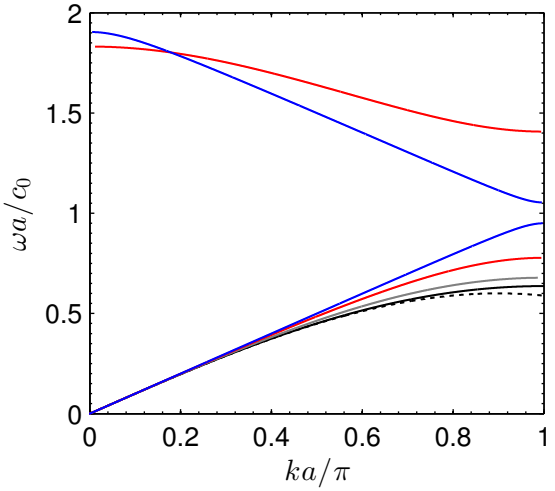


Figure 2.35: Dispersion relation for the layered media using $c_2/c_1 = 0.1$ and $\alpha = 0.1$ (blue), $\alpha = 0.5$ (red) and $\alpha = 0.9$ (gray), mono-atomic lattice (black) and the KdV homogeneous limit (dotted line). It can be observed that the layered linear dispersion relation converges to the lattice dispersion for small inclusion of low sound speed.

case of the mono-atomic chain dispersion (gray line in Fig. 2.35), to situations in which infinitesimal bandgap are created and the group speed is c_0 for all the frequencies (blue line in Fig. 2.35).

As can be seen, the layered media dispersion can modify its shape in a large amount of different configurations. Soliton shape, width and amplitude will depend in those parameters.

Let us recall here the second order lossless-Westervelt Eq. (2.31), assuming ρ_0 does not change with space and for plane waves travelling in the x direction

$$\frac{\partial^2 p}{\partial t^2} - c_0^2 \frac{\partial^2 p}{\partial x^2} - \frac{\beta}{\rho_0 c_0^2} \frac{\partial^2 p^2}{\partial t^2} = 0. \tag{2.63}$$

Here, as usual in the literature[6], we introduce the "travelling" coordinate system $z = x - c_0 t$ in which the reference frame z moves "with the wave" at speed c_0. Also, we define the new slow changing $\tau = t$ that corresponding to the travelling coordinates. The changes in the new coordinates can be related to the standard ones as

$$\frac{\partial}{\partial x} = \frac{\partial}{\partial z} \quad , \quad \frac{\partial}{\partial t} = \frac{\partial}{\partial \tau} - c_0 \frac{\partial}{\partial z} \tag{2.64}$$

[6] Although for boundary problems is more convenient to transform the reference frame to a "retarded time" coordinate, we introduce the spatial "travelling" coordinates for convenience. The transformation here would be more appropriate for initial value problems.

After some algebra, substitution of Eqs. (2.64) in Eq. (2.63) yields the lossless version of the Burgers equation

$$\frac{\partial p}{\partial \tau} + \frac{\beta}{\rho_0 c_0} p \frac{\partial p}{\partial z} = 0, \tag{2.65}$$

where the term $\partial^2 p/\partial \tau^2$ has been neglected due to the slowness change in the time τ. This equation can be rewritten in terms of particle velocity using the first order relation $v \approx p/\rho_0 c_0$ as

$$\frac{\partial v}{\partial \tau} + \beta v \frac{\partial v}{\partial z} = 0. \tag{2.66}$$

That is actually more close to its original form derived by Burgers. For convenience, let us return again to the static reference coordinate system, where Eq. (2.66), can be expressed as

$$\frac{\partial v}{\partial t} - (c_0 + \beta v) \frac{\partial v}{\partial x} = 0. \tag{2.67}$$

In this evolution equation is clearly evident amplitude dependence of the wave speed $c = c_0 + \beta v$, causing the well known steepening of the waveforms. As in previous sections, we know that the layered dispersion arises from the solution of the linearized wave equation with the layered media boundary conditions, where the eigenvalue problem leads to the Rytov's dispersion relation Eq. (2.1). In order to model KdV type dispersion, $\omega = c_0 k - b k^3$, an additional term can be introduced into the Eq. (2.67):

$$\frac{\partial v}{\partial t} - (c_0 + \beta v) \frac{\partial v}{\partial x} + b \frac{\partial^3 v}{\partial x^3} = 0\,. \tag{2.68}$$

With this term, the leading equation (in traveling coordinates) is the KdV equation, the most widely model for nonlinear waves in dispersive media. One of the exacts solution of the KdV equation is the solitary wave

$$v\,(x,t) = A \mathrm{sech}^2\left(\gamma\,(x - Vt)\right), \tag{2.69}$$

where the soliton width, γ, the amplitude, A, ant its speed, V, are related as

$$\gamma = \sqrt{\frac{\beta A}{12 b}}\,, \tag{2.70}$$

$$V = c_0 + \frac{\beta A}{3} \tag{2.71}$$

Here and beyond, we will demonstrate numerically the existence of this solution in the layered media, showing its limits of validity. Furthermore, we will investigate the behavior of solitary waves in the regime in which the layered media dispersion cannot be described by a KdV model with accuracy.

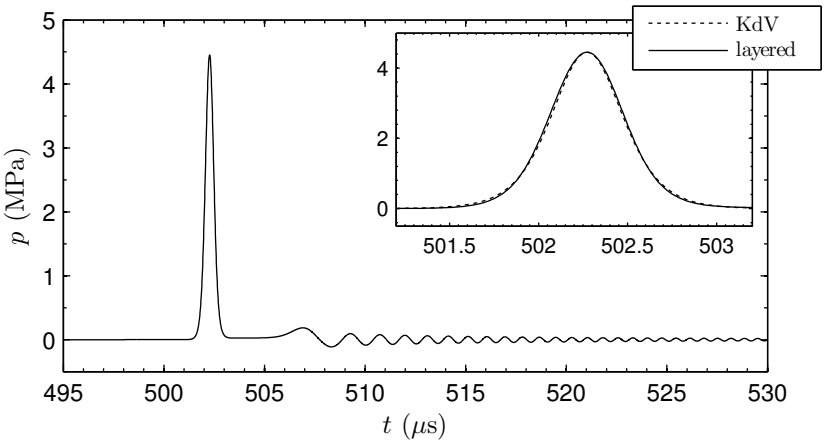


Figure 2.36: Solitary wave for the layered parameters $c_2/c_1 = 0.1$ and $\alpha = 0.1$, (continuous line) numerical solution of the layered media (dotted line) KdV solution.

Figure 2.36 shows the evolution of solitary waves for the layered parameters $c_2/c_1 = 0.1$ and $\alpha = 0.1$. As shown previously in Fig. 2.35, in this regime of parameters the layered dispersion can be described precisely by the KdV dispersive model. Due to both models are not exactly the same (even for the mono-atomic chain this is not fulfilled), we cannot claim the solitary wave solution observed in the layered system is strictly described by the solitary solution Eq. (2.69). However, as can be seen from the numerical tests, both solution closely agrees.

2.6.2 Non-cubic dispersion solitons

The presented KdV-like soliton exist only for a particular set of condition. In general, the dispersion near the band gap cannot be accurately described by the KdV dispersion. Furthermore, in case of high-amplitude/low-width solitary waves, the soliton spectrum can reach superior bands, that are in-existent in the KdV model. Here, we briefly present the existence of solitons with its width comparable to the lattice separation. Figure 2.37 shows four examples of propagating localized waves with different amplitudes. As can observed, as the soliton amplitude increases its speed increases and its width reduces, as commonly observed is any solitary wave. However, it can be seen that for high amplitude solitons, in which the width of the localized wave is of the order of the lattice, there exist remarkable differences with the continuum KdV approximation. In this simulations, the initial excitation is the KdV solution. Thus, for the low amplitude regime (Fig. 2.37 (a)) the soliton solution matches the excitation and propagates without changing its shape, amplitude and velocity. However, for higher amplitudes (Fig. 2.37 (b, c)) , it can be observed that the KdV is not the exact solution: the solitary wave breaks into

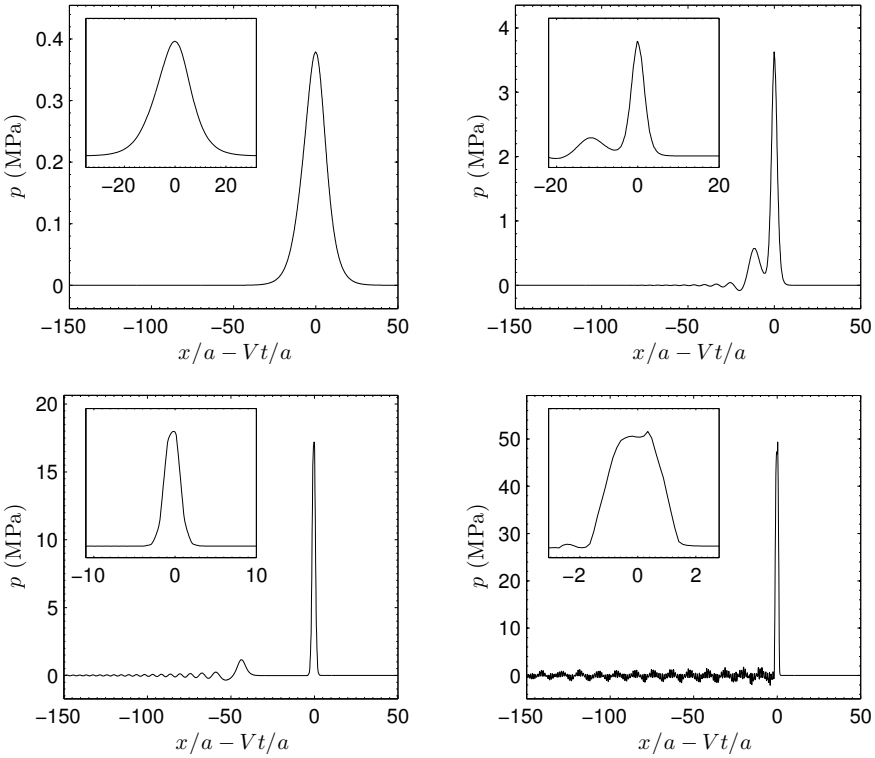


Figure 2.37: Examples of 4 solitons with increasing amplitudes.

other wave-packets plus an oscillatory tail that its left behind. Finally, in the regime width the soliton spectrum extend over the band-gap and up to second band, i.e. for very localized waves waves (Fig. 2.37 (d)) , the solitary wave suffers from a process of radiation. Note this radiation is totally different from the oscillatory tail shown in Figs. 2.37 (b, c): this radiation is not left behind and the localized wave continuously radiate low linear waves or phonons on its tail.

On the other hand, Fig. 2.38 shows the space time diagram of these waves. It can be seen clearly how the speed increases from c_0 to V, being V the speed of the localized wave. Here, the radiation is not visible due to the scaling of the color map but another particular feature of this system can be observed. For high amplitude solitons, the amplitude oscillates periodically in time and space, showing variations that in space matches the lattice period a and in time Vt/a. Therefore, the main features of the solitons in the discrete limit, where the width of the wave is comparable to the layer thickness is the existence of tail radiation and periodic oscillatory amplitude of the strongly localized waves.

A more detailed study is presented in Fig. 2.39, where we show the amplitude

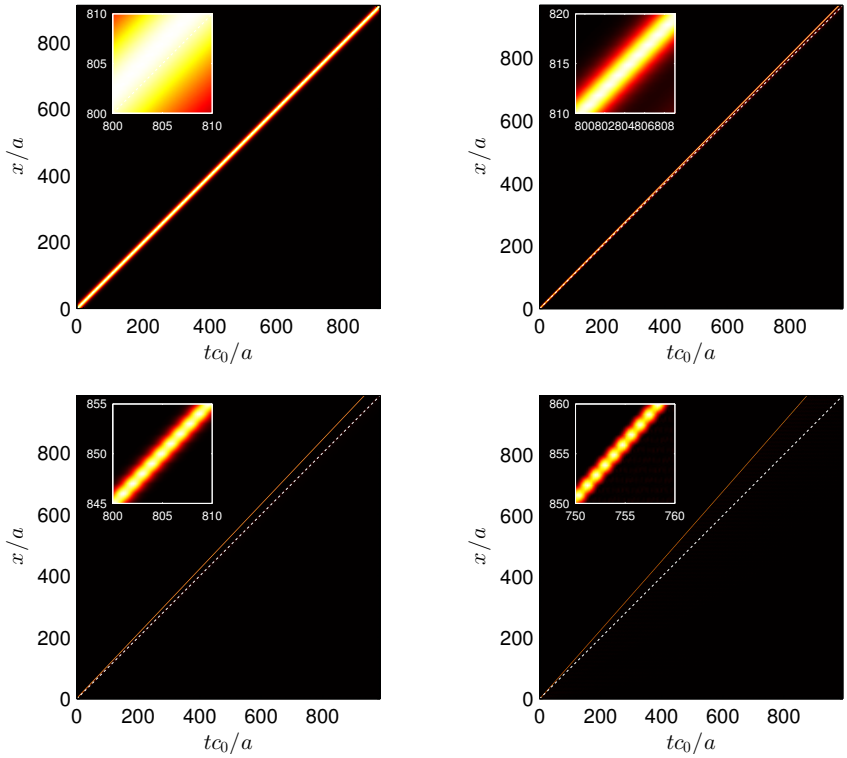


Figure 2.38: Space-time diagram representation of the solitons in Fig. 2.37, with increasing amplitude and velocity.

dependence of the soliton amplitude in function of its velocity. It can be seen that the KdV regime is only valid for weakly nonlinear excitations, of in other words, for wide solitons. For amplitudes of several MPa[7] the soliton velocity observed in simulations is considerably higher than in the KdV model.

2.6.3 1D Layered chirped: progressive amplification of solitons

The layered media offers the possibility of artificially modify the dispersion relation. As seen in previous sections, the modification of the lattice parameters can be made adiabatically, increasing or decreasing the lattice period progressively with distance forming chirped layered structure. Along the solitary wave amplitude, speed an thickness depends on the dispersion, the chirped la provides an usefully way to progressively amplify solitons. Thus, we present a test of this idea where

[7]The lattice parameters were $a = 0.85$, $c_2 = 1500$ m/s, $c_1 = 450$ m/s and $d = 0.225$ mm

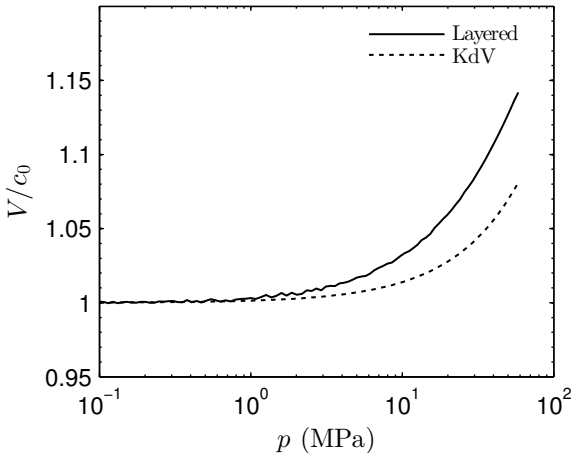


Figure 2.39: Soliton speed as a function of its amplitude for (continuous line) numerical results and (dotted line) KdV solution.

a chirped lattice period decreases with distance.

The initial excitation at the beginning of the lattice is a wide, KdV-type excitation. Thus, as Fig. 2.40 shows, soliton start to propagate at a supersonic, but low speed. As long the period is decreased, the dispersion seen by the wave adiabatically changes. Thus, the solitary wave solution slowly adapts it amplitude and thick according to the local dispersion. The result is that the wave can be stretched, amplified and accelerated to higher supersonic speeds. This proof of concept provides a method to manage the parameters of localized waves that can be applied to any other lattice. Configurations of special interest are probably the dispersion management of strain solitons in micro-structured composites, high intensity ultrasonic cutting devices for medical applications triggered by trains of amplified and pulsed excitations (instead of continuous mode) to reduce the heating and material fatigue (Harvey et al., 2014), or even period-varying granular beads composed of metallic spheres for drilling devices that can be usefully planetary exploration (Harkness et al., 2012).

2.7 Conclusions

In this Chapter we have analyzed the nonlinear propagation of acoustic waves in a layered media. The harmonic generation processes are presented and discussed mainly with numerical solutions considering a fluid-fluid structure. The strong characteristic dispersion of a layered media, in addition to the fluid nonlinearity, provides a wide range of possibilities for harmonic generation and control. In this

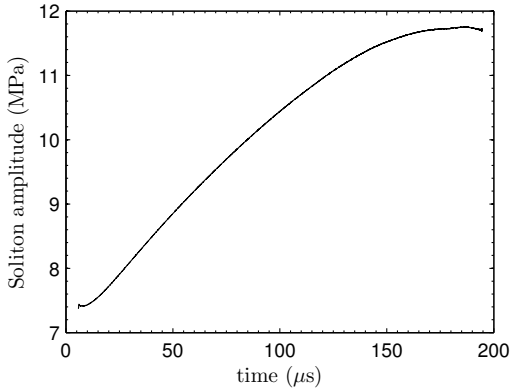


Figure 2.40: Progressive amplification of a soliton traveling in a chirped lattice.

sense, the effective nonlinearity of the composite media can be tuned for obtaining the desired harmonic balance. We provide the methods for selective harmonic generation, where the material layers can be adjusted for generate only second harmonic, only third harmonic, discard the even harmonics creating a cubic-nonlinear medium composed of quadratically-nonlinear layer. We provided also conditions for fabrication of waveguides for intense acoustic waves with extraordinary nonlinear distortion. Finally, the layered media provides conditions for dispersion management solitons, that are briefly presented, extending the work existent in the literature to the discrete limit of the soliton in which the width is of the order of the media periodicity.

On the other hand, much work on modeling the presented results remains. In this sense, we are currently working on Coupled Mode Theory. This analytical method widely used in optics (Malomed, 2000) can provide simple explanation of the dynamics of the system in terms of forward and backward coupled fields for fundamental and higher harmonics.

References

Albin, Nathan and Oscar P. Bruno (2011). "A spectral FC solver for the compressible Navier Stokes equations in general domains I: Explicit time-stepping". In: *J. Comput. Phys.* 230.16, pp. 6248–6270.

Botteldooren, D. (1996). "Numerical model for moderately nonlinear sound propagation in three-dimensional structures". In: *J. Acoust. Soc. Am.* 100.3, pp. 1357–1367.

Boussinesq, Joseph (1877). *Essai sur la théorie des eaux courantes*. Vol. 2. Imprimerie nationale.

Boussinesq, Joseph Valentin (1871). "Théorie générale des mouvements qui sont propagés dans un canal rectangulaire horizontal". In: *CR Acad. Sci. Paris* 73, pp. 256–260.

Brillouin, L. (2003). *Wave Propagation in Periodic Structures: Electric Filters and Crystal Lattices*. Dover phoenix editions. Dover Publications.

Cheng, YC, S Kicas, J Trull, M Peckus, C Cojocaru, R Vilaseca, R Drazdys, and K Staliunas (2014). "Flat Focusing Mirror". In: *Scientific reports* 4, pp. –.

Fainstein, Alejandro, N Daniel Lanzillotti-Kimura, Bernard Jusserand, and B Perrin (2013). "Strong optical-mechanical coupling in a vertical GaAs/AlAs microcavity for subterahertz phonons and near-infrared light". In: *Physical review letters* 110.3, p. 037403.

Ginter, Siegfried, Marko Liebler, Eckard Steiger, Thomas Dreyer, and Rainer E. Riedlinger (2002). "Full-wave modeling of therapeutic ultrasound: nonlinear ultrasound propagation in ideal fluids." In: *J. Acoust. Soc. Am.* 111.5, pp. 2049–2059.

Gurbatov, S.N., O.V. Rudenko, and A.I. Saichev (2011). "Waves and Structures in Nonlinear Nondispersive Media. General Theory and Applications to Nonlinear Acoustics". In: ed. by S.N. Gurbatov, O.V. Rudenko, and A.I. Saichev. Springer. Chap. Chapter 8. Types of Acoustic Nonlinearities and Methods of Nonlinear Acoustic Diagnostics, pp. 271–304.

Hamilton, Mark F, David T Blackstock, et al. (1998a). *Nonlinear acoustics*. Vol. 237. Academic press San Diego.

Harkness, Patrick and Margaret Lucas (2012). "A brief overview of space applications for ultrasonics". In: *Ultrasonics* 52.8, pp. 975–979.

Harvey, Gerald, Anthony Gachagan, and Tapiwa Mutasa (2014). "Review of high-power ultrasound-industrial applications and measurement methods". In: *Ultrasonics, Ferroelectrics and Frequency Control, IEEE Transactions on* 61.3, pp. 481–495.

Huynh, A, ND Lanzillotti-Kimura, B Jusserand, B Perrin, A Fainstein, MF Pascual-Winter, E Peronne, and A Lemaître (2006). "Subterahertz phonon dynamics in acoustic nanocavities". In: *Physical review letters* 97.11, p. 115502.

Huynh, Agnes, B Perrin, and A Lemaître (2015). "Semiconductor superlattices: A tool for terahertz acoustics". In: *Ultrasonics* 56, pp. 66–79.

Jacob, Xavier, Stefan Catheline, Jean-Luc Gennisson, Christophe Barrière, Daniel Royer, and Mathias Fink (2007). "Nonlinear shear wave interaction in soft solids". In: *The Journal of the Acoustical Society of America* 122.4, pp. 1917–1926.

Kordeweg, DJ and G de Vries (1895). "On the change of form of long waves advancing in a rectangular channel, and a new type of long stationary wave". In: *Phil. Mag* 39, pp. 422–443.

Kosevich, Arnold M. (2005). "The Crystal Lattice: Phonons, Solitons, Dislocations, Superlattices, Second Edition". In: *The Crystal Lattice*. Ed. by Arnold M. Kosevich. Wiley-VCH Verlag GmbH & Co. KGaA. Chap. Chapter 5. Acoustics of Elastic Superlattices: Phonon Crystals, pp. 153–162.

Liang, Bin, Bo Yuan, and Jian-chun Cheng (2009). "Acoustic diode: Rectification of acoustic energy flux in one-dimensional systems". In: *Physical review letters* 103.10, p. 104301.

Malomed, Boris A (2000). "Solitons in optical media with quadratic nonlinearity". In: *Nonlinear Science at the Dawn of the 21st Century*. Springer, pp. 247–262.

Maryam, W, AV Akimov, RP Campion, and AJ Kent (2013). "Dynamics of a vertical cavity quantum cascade phonon laser structure". In: *Nature communications* 4.

Naugolnykh, K. and L. Ostrovsky (1998). *Nonlinear Wave Processes in Acoustics*. Cambridge Texts in Applied Mathematics. Cambridge University Press.

Rayleigh, Lord (1876). "On waves". In: *Phil. Mag* 1.5, pp. 257–279.

Romero-García, Vicente, R Picó, A Cebrecos, Víctor José Sánchez-Morcillo, and K Staliunas (2013). "Enhancement of sound in chirped sonic crystals". In: *Applied Physics Letters* 102.9, p. 091906.

Rudenko, O.V. and S.I. Soluian (1977). *Theoretical foundations of nonlinear acoustics*. Studies in Soviet science. New York, NY 10011, USA: Consultants Bureau, p. 274.

Russell, J Scott (1844). "Report on waves". In: *14th meeting of the British Association for the Advancement of Science*. Vol. 311, p. 390.

Sánchez-Morcillo, V., I. Pérez-Arjona, V. Romero-García, V. Tournat, and V. Gusev (2013). "Second-harmonic generation for dispersive elastic waves in a discrete granular chain". In: *Physical Review E* 88.4, p. 043203.

Santosa, Fadil and William W Symes (1991). "A dispersive effective medium for wave propagation in periodic composites". In: *SIAM Journal on Applied Mathematics* 51.4, pp. 984–1005.

Tournat, V, VE Gusev, V Yu Zaitsev, and B Castagnede (2004). "Acoustic second-harmonic generation with shear to longitudinal mode conversion in granular media". In: *Europhysics Letters* 66.6, p. 798.

Vanhille, Christian and CleofCampos-Pozuelo (2004). "Numerical simulation of two-dimensional nonlinear standing acoustic waves". In: *J. Acoust. Soc. Am.* 116.1, p. 194.

Yong, Darryl H and Randall J LeVeque (2003). "Solitary waves in layered nonlinear media". In: *SIAM Journal on Applied Mathematics* 63.5, pp. 1539–1560.

Yun, Y, GQ Miao, P Zhang, K Huang, and RJ Wei (2005). "Nonlinear acoustic wave propagating in one-dimensional layered system". In: *Physics Letters A* 343.5, pp. 351–358.

Zabusky, Norman J and Martin D Kruskal (1965). "Interaction of solitons in a collisionless plasma and the recurrence of initial states". In: *Phys. Rev. Lett* 15.6, pp. 240–243.

Publications

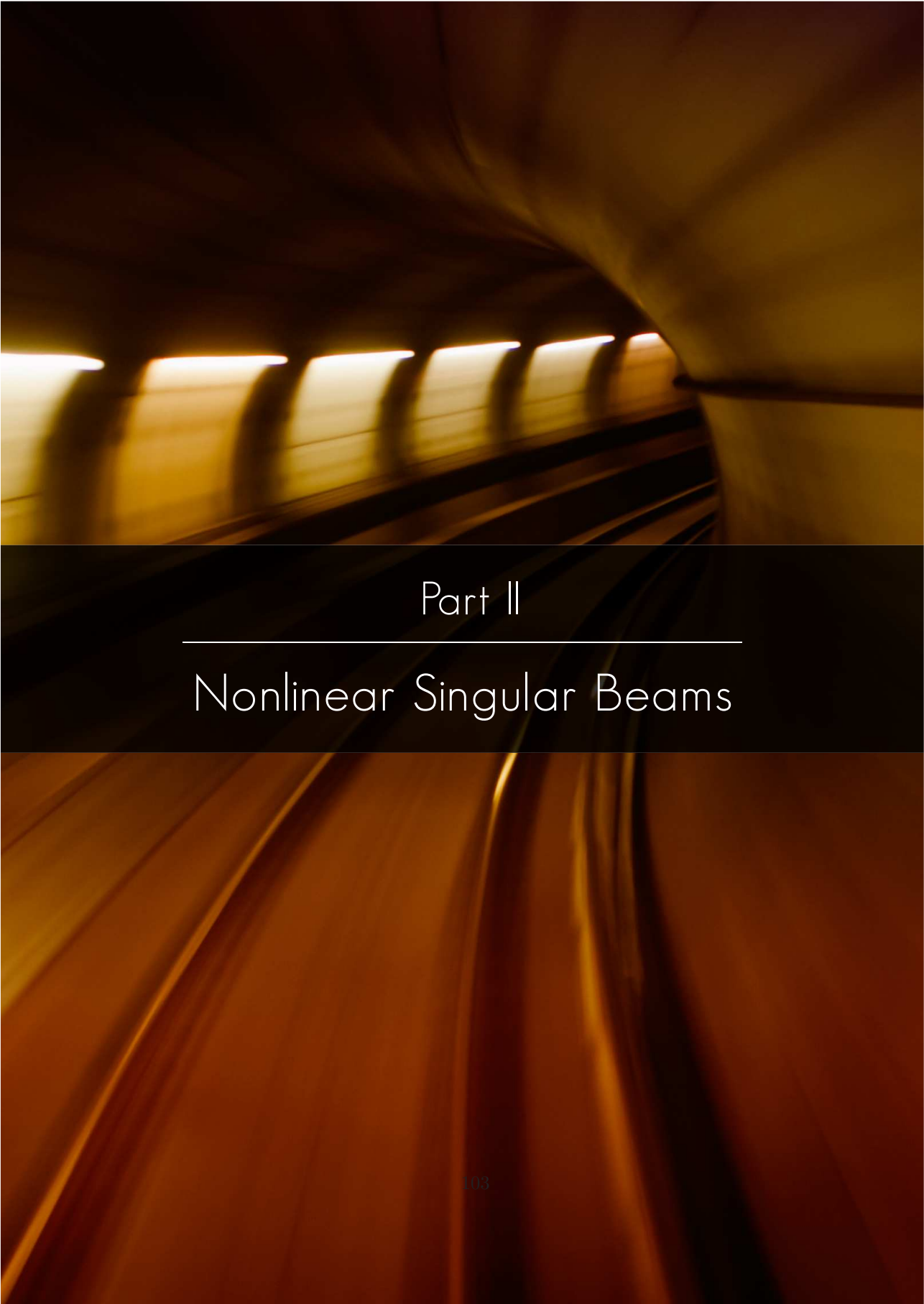
The contents of this chapter has been presented in the following publications:

Journal papers

- **Jiménez, N.**, Mehrem, A., Picó, R., García-Raffi, L. M., Sánchez-Morcillo, V. J. "Nonlinear propagation and control of acoustic waves in phononic superlattices" *Comtes Rendus Physique : Special issue on phononic crystals*, Elsevier. *Submitted* 19 May (2015).

Conference proceedings

- V.J. Sánchez-Morcillo, **N. Jiménez**, A. Mehrem, R. Picó, Ll. García-Raffi, V. Romero-García, V. Tournat. "Nonlinear waves in periodic media: from lattices to superlattices and phononic crystals". *PHONONICS 2015: 3nd International Conference on Phononic Crystals/Metamaterials, Phonon Transport and Phonon Coupling.* Paris, France. May 31–June 5 (2015)
- V. J. Sánchez-Morcillo, **N. Jimenez**, A. Mehrem, E.M. HamHam, L. García-Raffi and R. Picó. "Propagation of Intense Acoustic Waves in Sonic Crystals", *ICU 2015: International Congress on Ultrasonics.* Metz, France. May 11-14 (2015)
- Mehrem, A., Hamham, E. M., **Jiménez, N.**, Cebrecos, A., Pico, R.; Sanchez-Morcillo, V. and García-Raffi, L. M. "Nonlinear Acoustic Waves Periodic Media" *7th Forum Acusticum 2014.* Krakow, Poland. September 7 (2014)



Part II

Nonlinear Singular Beams